STRUCTURAL HEALTH MONITORING AND FAULT DIAGNOSIS

BASED ON ARTIFICIAL IMMUNE SYSTEM

by

Wenchang Xiao

A Thesis

Submitted to the Faculty

of the

WORCESTER POLYTECHNIC INSTITUTE

in partial fulfillment of the requirements for the

Degree of Master of Science

in

Mechanical Engineering

by

_____

February 2012

APPROVED:

_____

Professor Zhikun Hou, Major Advisor

_____

Professor Mikhail F. Dimentberg, Committee Member

_____

Professor Yeesock Kim, Committee Member

_____

Professor Stephen S. Nestinger, Graduate Committee Representative

Abstract

This thesis presents a development of Structural Health Monitoring (SHM) and Fault Diagnosis based on Artificial Immune System (AIS), a biology-inspired method motivated from the Biological Immune System (BIS). Using the antigen to model structural health or damage condition of specific characteristics and the antibody to represent an information system or a database that can identify the specific damage pattern, the AIS can detect structural damage and then take action to ensure the structural integrity. In this study the antibodies for SHM were first trained and then tested. The feature space in training includes the natural frequencies and the modal shapes extracted from the simulated structural response data including both free-vibration and seismic response data. The concepts were illustrated for a 2-DOF linear mass-spring-damper system and promising results were obtained. It has shown that the methodology can be effectively used to detect, locate, and assess damage if it occurred. Consistently good results were obtained for both feature spaces of the natural frequencies and the modal shapes extracted from both response data sets. As the only exception, some significant errors were observed in the result for the seismic response data when the second modal shape was used as the feature space. The study has shown great promises of the methodology for structural health monitoring, especially in the case when the measurement data are not sufficient. The work lays a solid foundation for future investigations on the AIS application for large-scale complex structures.

Acknowledgments

I would like to show my deepest gratitude to my honorable advisor, Dr. Zhikun Hou, a respectable, responsible and resourceful scholar, who has provided me with valuable guidance in every stage of the writing of this thesis. In academic, he introduced me to the world of mechanical vibration, and extended to the areas of Structural Health Monitoring and Artificial Immune System. In writing, he has checked through my thesis with patience and given me instructive suggestions, and he also played an important role in indicating a bright road in my future writing.

I would like to thank Yue Wang and Lili Yuan for helping me with Matlab skills. Yue Wang helped me to solve a lot of fundamental problems at the beginning of my research, and Lili Yuan gave me important suggestions for the problems about vibration signal analysis. They promoted the progress of my research. I would also like to thank Xiao'an Yan and Yao Wang, who have given me suggestions and encouragement.

Additionally, I would like to give my special thank to my family. Without my parents and my uncle and aunt, I cannot study abroad and finish this thesis. Last but not least, I'd like to thank all my friends, for their friendship and suggestions, they constantly encouraged me when I felt frustrated with problems in this thesis.

Contents

List of figures

List of tables

1 Background

1.1 Structural Health Monitoring

The process of implementing a damage detection and characterization strategy for engineering structures is referred to as Structural Health Monitoring (SHM) [1] to ensure the structural safety and functionality. A SHM process involves the periodical observation of sampled dynamic response measurements from sensors, and the analysis of the measurement data to determine the current state of structural health condition that, for long-term SHM, can be periodically updated to assess the structural ability to perform its intended function in light of the inevitable aging and degradation resulting from operational environments. [2]

SHM has been developed in various engineering disciplines as a powerful tool detect, locate and assess damage, if it occurs, which may lay a solid foundation for an appropriate maintenance decision. SHM is especially useful for detecting invisible damage, such as those occurred in civil infrastructures after a severe earthquake. To ensure the structural safety, engineers may need to inspect joints of structures for possible damage after a seismic event, which may require extensive removal of nonstructural material, and put (at least part of) the structure out of service during inspection. [3]

Millions of building structures need routine maintenance to inspect and, if needed, to repair for the structural integrity, especially those aging and deteriorating to their design life. Nondestructive testing is sometimes required for assessment of a critical structural component inside a complex structural system. However, the scope of nondestructive testing may be limited and also it might be prohibitively costly. In contrast to the costly manual inspection and non-destructive testing, the SHM may provide economic and reliable alternative to consistently assess the structural health condition for necessary maintenance decision

In recent years, SHM, as an effective, economic and reliable approach, was used for many structures including bridges, dams, and high-rising buildings. For example, a sophisticated bridge monitoring system named as Wind and Structural Health Monitoring System (WASHMS) was installed in the the Tsing Ma[4], Ting Kau, and Kap Shui Mun bridges[5] that run between Hong Kong and the Hong Kong Airport. Similar systems for large-scale structures have been developed in Europe[6–9], the United States[10,11], Canada[12,13], Japan[14,15], Korea[16,17], China[5,18,19] and other countries[20–22].

SHM is also used on the greatest dam, the Three Gorges Dam [23], in China since 2002. Other SHM applications are exemplified by the SHM system on a 24-floor building in San Francisco to monitor its seismic performance [24] and development of built-in sensor network for aerospace structures [25].

1.2 Modal analysis for linear discrete systems

The feature spaces using in the AIS-based SHM in the thesis scheme are the natural frequencies and modal shapes, the physical quantities sensitive to structural damage. These quantities are extracted from the structural response data simulated by model analysis, a well-known technique in vibration engineering to solve for an initial value problem (IVP) for vibrational responses of a linear structural system based on the principle of modal superposition. Modal analysis also bring some great insight in data mining and interpretation. This section provides a brief summary of the modal analysis. For a linear MDOF vibration system, the IVP (initial-value problem) in matrix form is given by:

$$M\underline{\ddot{x}} + C\underline{\dot{x}} + K\underline{x} = \underline{F} \tag{1.1a}$$

$$\underline{x}(0) = \underline{x}_0 \tag{1.1b}$$

$$\underline{\dot{x}}(0) = \underline{v}_0 \tag{1.1c}$$

where M is the mass matrix, C is the viscous damping matrix, and K is the stiffness matrix. The size of all matrices is N x N where N is the number of degree-of-freedom (DOF) of the MODF system. The displacement vector $\underline{x}$ and the external forces vector $\underline{F}$ are N×1 vectors. $\underline{x}_0$ is the vector of the specified initial positions, and $\underline{v}_0$ is the vector of the specified initial velocities.

To solve the IVP by the modal analysis technique, it is usually to solve the associated

eigenvalue problem first to find the natural frequencies ω_i and the corresponding normal modes $\underline{X}^{(i)}$ ($1 \leq i \leq N$). Viewing the physical response is superposition of the N modal responses, the solution vector can be written as:

$$\underline{x} = \eta_1(t)\underline{X}^{(1)} + \eta_2(t)\underline{X}^{(2)} + \cdots + \eta_N(t)\underline{X}^{(N)} = \Phi\underline{\eta}(t) \tag{1.2}$$

where $\eta_1(t)$, $\eta_2(t)$, ..., $\eta_N(t)$ are time-dependent generalized coordinates, also known as the principal coordinates or modal participation coefficients. By defining a modal matrix Φ in which the j-th column is the modal shape vector $\underline{X}^{(j)}$--that is:

$$\Phi = [\underline{X}^{(1)} \ \underline{X}^{(2)} \ \dots \ \underline{X}^{(N)}] \tag{1.3}$$

(1.1a) can be rewritten as:

$$\Phi^T M \Phi \ddot{\eta} + \Phi^T C \Phi \dot{\eta} + \Phi^T K \Phi \eta = \Phi^T \underline{F} \tag{1.4a}$$

Using the orthogonal property of the modal matrix with respect to M and K and the assumption of classical damping, one obtains:

$$\Phi^T M \Phi = \begin{pmatrix} \ddots & & 0 \\ & m_i & \\ 0 & & \ddots \end{pmatrix} \quad \Phi^T K \Phi = \begin{pmatrix} \ddots & & 0 \\ & k_i & \\ 0 & & \ddots \end{pmatrix} \quad \Phi^T C \Phi = \begin{pmatrix} \ddots & & 0 \\ & c_i & \\ 0 & & \ddots \end{pmatrix} \tag{1.4b}$$

$$\underline{p} = (\cdots \quad p_i \quad \cdots)' = \Phi^T \underline{F}. \tag{1.4c}$$

Thus the original coupled equations of motions are transformed into a set of uncoupled N SDOF systems:

$$m_i \ddot{\eta}_i + c_i \dot{\eta}_i + k_i \eta_i = p_i(t) \ (i = 1, 2, \dots, N) \tag{1.5a}$$

On the other hand, (1.1b) can be rewritten in this form:

$$\underline{\eta}(0) = \Phi^{-1}\underline{x}(0) = \underline{\eta}_0 \tag{1.4c}$$

$$\underline{\dot{\eta}}(0) = \Phi^{-1}\underline{\dot{x}}(0) = \underline{\dot{\eta}}_0 \tag{1.4d}$$

which define the initial conditions for the modal responses, i.e.

$$\eta_i(0) = \eta_{i0}, \dot{\eta}_i(0) = \dot{\eta}_{i0} \ (i = 1, 2, \dots, N) \tag{1.5b}$$

By the modal decomposition, the IVPs of the set of uncoupled N SDOF systems are obtained as:

$$m_i\ddot{\eta}_i + c_i\dot{\eta}_i + k_i\eta_i = p_i(t) \tag{1.6a}$$

$$\eta_i(0) = \eta_{i0}, \dot{\eta}_i(0) = \dot{\eta}_{i0} \tag{1.6b}$$

$$(i = 1, 2, \dots, N)$$

Solve these IVPs, and substitute the solution $\eta_i(t)$ (i=1, 2, …, N) into (1.2), the solution of this MDOF system is then obtained.

1.3 Introduction to Artificial Immune System

1.3.1 Biological Immune System

The Biological Immune System (BIS) is a robust, complex, adaptive system of biological structures and processes within an organism that protects against disease by isolating and killing the non-self cells or molecules.[26,27] The Artificial Immune System (AIS) imitated from BIS.

In order to have a preliminary understanding of BIS, the most important terms: antigen and antibody should be mentioned first. An antibody is a protein used by the immune system to identify and neutralize foreign objects such as bacteria and viruses. An antigen is a cell or molecule that, when introduced into the body, triggers the production of an antibody by the immune system, which might be the non-self cell and molecule, or mutated self-cell and molecule. [28, 29] Fig.1.1 shows 6 kinds of antigens and 1 kind of antibody. Each antibody binds to a specific antigen at the end of the antibody, an interaction similar to a lock and key.
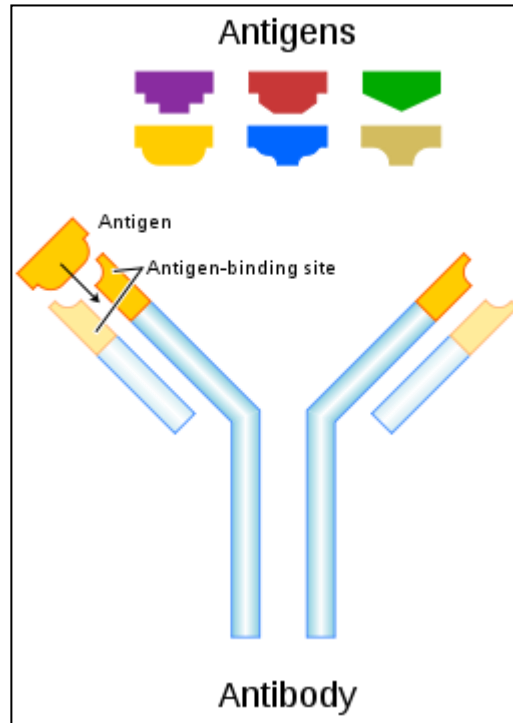
Fig.1.1 Each antibody binds to a specific antigen like a lock and key. [30]

There are three phases in the adaptive immunity: phase sensitization, phase proliferation and differentiation, and phase effect. In the first phase (I, II, and III in Fig.1.2), antigens are identified by the immune cells. Then the immune cells are activated and proliferated in the second phase (IV and V in Fig.1.2). In the same time, some of their offspring will become long-lived memory cells, which will remember each specific antigen encountered and can mount a strong response if the antigen is detected again throughout the lifetime of an animal. In the third phase (VI and VII in Fig.1.2), antibodies and some other things are produced and match with the antigens then kill them.
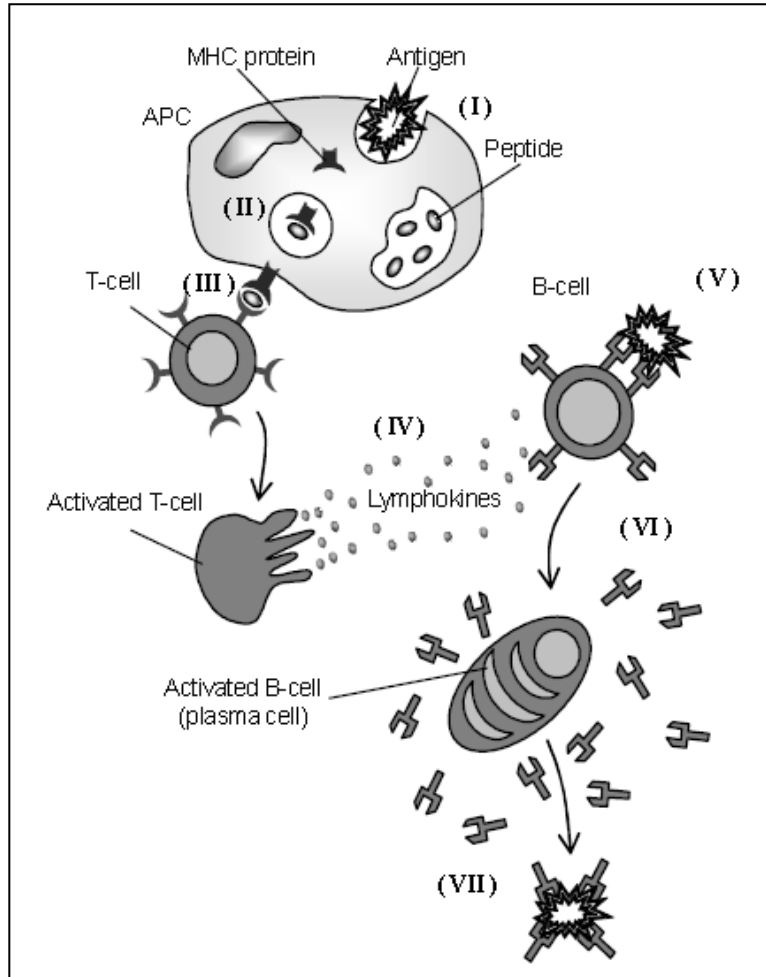
Fig.1.2 Pictorial representation of the essence of the acquired immune system mechanism.[31]

There are two important principles in biology: clone and negative selection. Cloning in biology is the process of producing similar populations of genetically identical individuals that occurs in nature when organisms such as bacteria, insects or plants reproduce asexually. Cloning in biotechnology refers to processes used to create copies of DNA fragments (molecular cloning), cells (cell cloning), or organisms.[31,32]

The negative selection deals with the immune system's ability to detect unknown antigens

while not reacting to the self cells. In general, T-cells that react against self-proteins are destroyed during the generation of them, thus, only those that do not bind to self-proteins are allowed to survive and proliferate.[31]

1.3.2 Artificial Immune System

Artificial Immune Systems (AIS) are computational systems inspired by the principles and processes of the vertebrate immune system. They are adaptive systems, inspired by theoretical immunology and observed immune functions, principles and models, which are applied to problem solving. [33] Fig.1.3 shows AIS is a branch of biology-inspired methods in Computational Intelligence field, which includes several algorithms. Clone and negative selection are used in this study and will be detailed later.
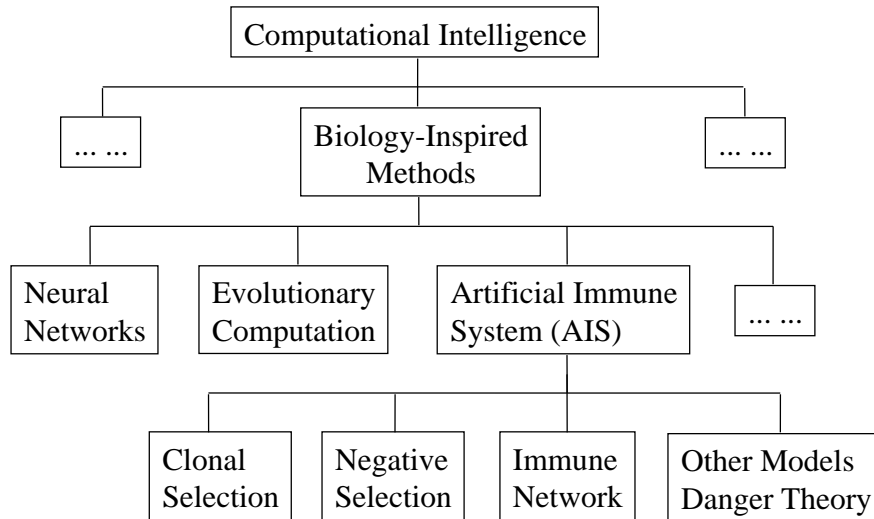
Fig.1.3 Artificial Immune System as a branch of Computational Intelligence. [34]

Like BIS, AIS also has its "antigen" and "antibody". From them, the concept of affinity is introduced in AIS. In AIS, the antigens are the information from the test. The antibodies are the detectors. The initial detectors are generated randomly, which will become matured detectors after a training process. Affinity is the dependence of the match-process between an antigen and an antibody defined as [35]:

$$\text{aff}(X, Y) = \frac{1}{1+d_E} \tag{1.7}$$

where X and Y are antigens and/or antibodies, and d_E is the Euclidean distance defined

as:

$$d_E = \sqrt{\sum_{i=1}^{N}(x_i - y_i)^2} \qquad (1.8)$$

where X=(x_1, x_2, …x_N), Y=(y_1,y_2,…,y_N).

Based on the literature [36], the concepts of AIS are related to those of BIS and their

correspondence can be found in Table 1. In this study, antigens are referred to structural

health or damage conditions with specific characteristics contained in the vibration

response measurement data; an antibody is a detector to be trained, and the group of

which after training provides a database, an information system for damage pattern

recognition; the process of mutate is a training procedure that leads initial raw detectors

to form a matures database capable to detect various damage patten..

Table 1 Comparison between BIS and AIS

BIS	AIS
Antigens	Structural health or damage conditions
An antibody	A detector of a specific damagepattern
The matured antibodies	Database or information system for damage detection
Recognition of antigens	Identification of health and damage conditions
Mutate process	Training procedure

Three immunological principles are primarily used in AIS methods, including the

immune network theory, the mechanisms of negative selection, and the clone selection

principles. The immune network theory is not involved in this thesis work. The other two

principles as explained as follow.

In AIS, the clonal selection principle follows the idea that only those cells that recognize

the antigen can proliferate. The main features of the clonal selection theory are:

- The new cells are copies of their parents (clone) subjected to a mutation mechanism
  with high rates;

- Elimination of newly differentiated lymphocytes carrying self-reactive receptors;

- Proliferation and differentiation on contact of mature cells with antigens.[37]

In Fig.1.4, there are 3 kinds of immune cells and only 1 kind of antigens. The cells that can

recognize the antigen will proliferate. The others will be eliminated. The selected cells will

differentiate to memory cells or be activated so that the antibodies can be produced.
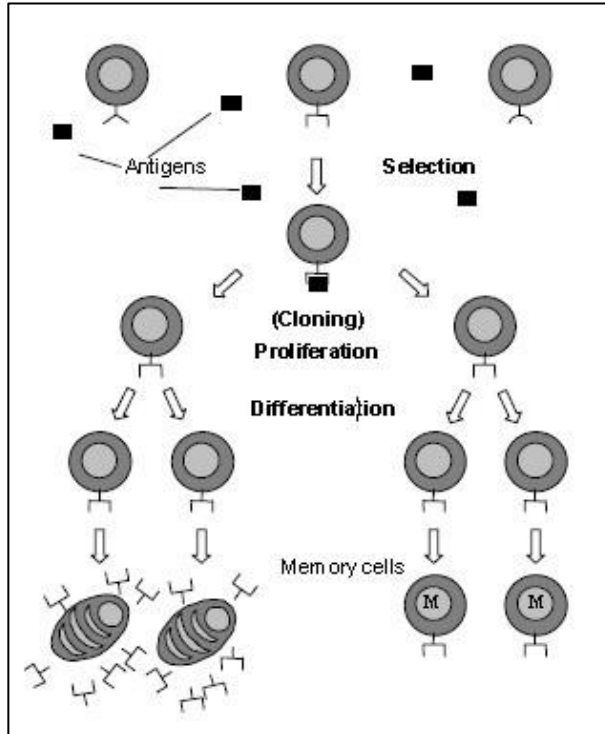
Fig.1.4 The clonal selection principle. [37]

Negative selection refers to the identification and deletion (apoptosis) of self-reacting cells that may select for and attack self tissues. To detect anomaly, it prepares a set of exemplar pattern detectors trained on normal (non-anomalous) patterns that model and detect unseen or anomalous patterns. [38] In Fig.1.5, there are two stages which show the main idea of negative selection. In generation stage, the detectors are generated by some random process. The initial detectors that match with healthy conditions are eliminated and the rest are kept and added to database. In the detection stage, the detectors in database are used to check whether an incoming data instance is self or non-self. If it matches any detector, then it is claimed as non-self or abnormal.
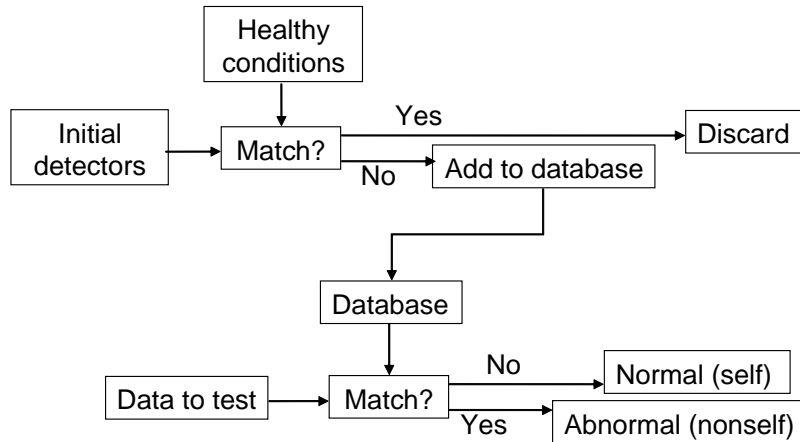
Fig.1.5 The basic concept of the Negative Selection (NS) Algorithm. [39]

Based on the literature [40-42], the common steps of Immune Algorithm (Fig.1.6) are:

I   Recognize antigens. The AIS affirms the incursion of the antigen. In this thesis, it refers to the process to get the data for the healthy condition and known damage patterns as specific antigens.

II   Generate the initial antibodies (detectors). The antibodies will be generated randomly.

III Calculate the affinity between the antigen and antibody.

IV   Termination conditions. Check the affinities, and if any affinity is out of the pre-set range, renew the antibody (step V), then do step III and re-check the new affinity until all the affinities are in the pre-set range.

V   Renew the antibody. If the affinity is out of the range, the antibody should be replaced by a new randomly-generated antibody.

```
        ┌─────────────────────┐
        │  Recognize antigens │
        └─────────────────────┘
                  │
                  ▼
┌────────────────────────────────────────┐
│ Generate the initial antibodies (detectors) │
└────────────────────────────────────────┘
                  │
                  ▼
        ┌─────────────────────┐
        │ Calculate the affinity │
        └─────────────────────┘
                  │
                  ▼
             Meet the              NO     ┌─────────────────────┐
           termination  ──────────────────▶│ Renew the antibody  │
           conditions?                     └─────────────────────┘
                  │
                 YES
                  │
                  ▼
             ┌────────┐
             │  End   │
             └────────┘
```
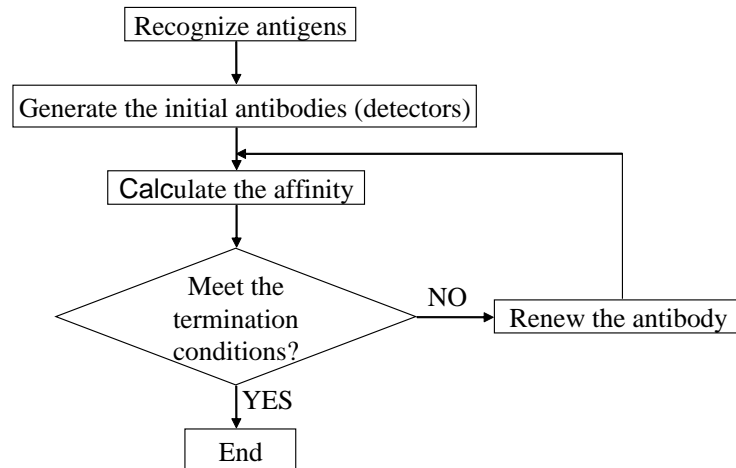
Fig.1.6 The algorithm flow chart of AIS.

The common steps of clone and negative selection and the common steps of Immune

Algorithm are not exactly alike. Based on the literature [37], the main steps of the Clonal

Selection Algorithm (Fig.1.7) are: (I) generate the initial antibodies (detectors), (II) select

best antibodies based on an affinity measure, (III) proliferate, (IV) differentiate, (V)

re-select and get the memory set, (VI) replace antibodies by the memory set.
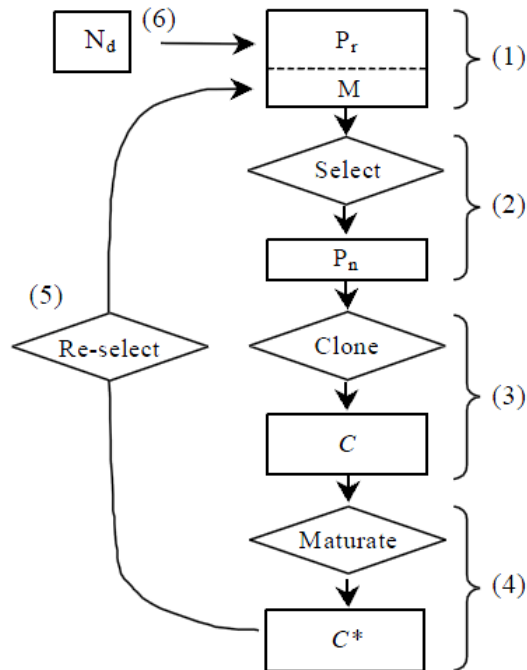
Fig.1.7 Block diagram of the clonal selection algorithm. [37]

Dipankar Dasgupta and Stephanie Forrest [43] present the negative selection algorithm steps as below:

I   Define self as a multiset S of strings of lengh l over a finite alphabet, a collection the we wish to protect or monitor. For example, S may be a segmented file, or a normal pattern of activity of some system or process.

II   Generate a set R of detectors, each of which fails to match any string in S. we partial matching rule, in which two strings match if and only if they are identical at least r contiguous positions, where r is a suitably chosen parameter.

III Monitor S for changes by continually matching the detectors against S. if any detector ever matches, a change (or deviation) must have occurred.[43]

AIS are being used in many applications such as anomaly detection, pattern recognition or image processing, data mining, computer security, optimal design, machine learning, adaptive control and fault diagnosis. The main applications can be found in computer security [44-48], adaptive control [49-53], and fault diagnosis [54-59].

Recently, some work is taken to develop AIS-based SHM. A representative work by Bo Chen (2009) is shown in Figure 1.8. [60] Experimental data from a benchmark structure proposed by the American Society of Civil Engineers are used in this research. The feature vectors are obtained by using an auto-regressive (AR) model of the time series for the simulated response data. While the damage is capable being detected as shown in Figure 1.8, the different patterns of damage seem not well separated. That might because of the complexity of the structure.
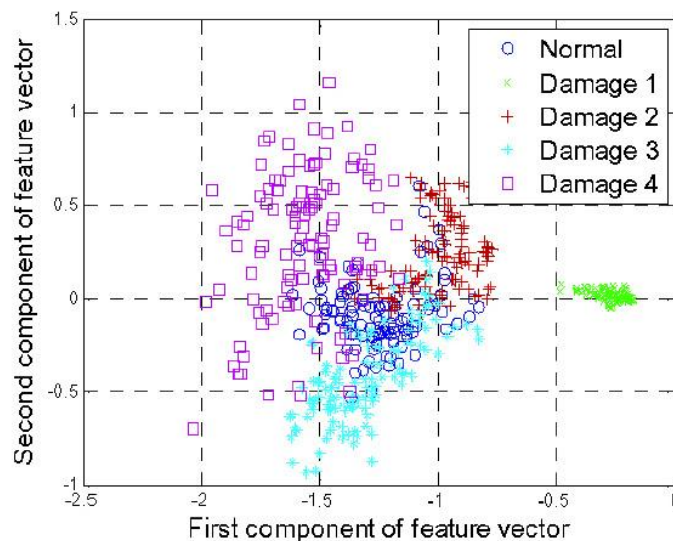
Fig.1.8 Normal and damage patterns form AIS-based SHM by Chen. [60]

2 AIS fault diagnosis

2.1 Basis of the AIS method

In this thesis, both normal condition and anomaly states are characterized by the N-dimensional state vector, which is normalized in such a way that all components take values in the interval [0, 1]. That is

$$V=(v_1, v_2, \ldots, v_N), (0 \leq v_i \leq 1, i=1, 2, \ldots, N). \tag{2.1}$$

In this chapter, N is the dimension of each state vector dimension. There are two kinds of antigens in this thesis. The first kind is the data from test before the structural damage, that is, in the normal/health condition and it is considered as the "self" information. The vector expression for one antigen of this kind is Vs:

$$V_s=(v_{s1}, v_{s2}, \ldots, v_{sN}), (0 \leq |v_{si}| \leq 1, i=1, 2, \ldots, N). \tag{2.2}$$

A set of the first kind of antigens is defined by:

$$G_1=\{ V_{s1}, V_{s2}, \ldots, V_{sK} \}. \tag{2.3}$$

Here, K is the number of state vector of the first kind of antigens in the set.

The second kind is the data from test after the structural damage, that is, in the abnormal condition, and it is considered as the "non-self" information. The vector expression for one antigen of this kind is Va:

$$V_a=(v_{a1}, v_{a2}, \ldots, v_{aN}), (0 \leq |v_{ai}| \leq 1, i=1, 2, \ldots, N). \tag{2.4}$$

A set of the second kind of antigens is defined as:

$$G_2 = \{ V_{a1}, V_{a2}, \ldots, V_{aL} \}. \tag{2.5}$$

Here, L is the number of state vector of the second kind of antigens in the set.

The antibodies are also the N-dimensional state vectors. The vector expression for one antibody is V_b:

$$V_b = (v_{b1}, v_{b2}, \ldots, v_{bN}), \ (0 \leq |v_{bi}| \leq 1, \ i=1, 2, \ldots, N). \tag{2.6}$$

A set of them is defined as:

$$D = \{ V_{b1}, V_{b2}, \ldots, V_{bM} \}. \tag{2.7}$$

Here, M is the number of state vector of the antibodies in the set.

The initial antibodies those work as detectors are generated randomly by computer simulation. Some of them will be able to match or partially match with the second kind of antigens G_2 and become matured antibodies after training, while the others will be discarded. As shown in Fig.2.1, there are two steps of training, the first is to separate antibodies associated with the healthy and damaged conditions and the second is to separate antibodies associated with different extents of damage, which will be dilated later in the part of AIS algorithm. The trained matured antibodies can later be used for damage detection/fault diagnosis. If there are any new response data, one may extract the feature space from the new data, calculate its affinity with the matured antibodies and assess the structural health condition.

```
                  ┌─────────────────────────────┐
                  │  Generated initial antibodies │
                  └─────────────────────────────┘
                                │
   ⎛      ⎞                      │      Training 1: separate healthy and
   │  G1  │──────────────────────┤              damaged  systems
   ⎝      ⎠                      │
                                ▼
                  ┌─────────────────────────────┐
                  │     Pretreated antibodies    │
                  └─────────────────────────────┘
                                │
   ⎛      ⎞                      │      Training 2: separate damages
   │  G2  │──────────────────────┤            wrt. extents & locations
   ⎝      ⎠                      │
                                ▼
                  ┌─────────────────────────────┐
                  │     Matured antibodies D     │
                  └─────────────────────────────┘
                                │
   ⎛           ⎞                 │
   │Data to test│────────────────┤      Fault diagnosis
   ⎝           ⎠                 │
                                ▼
                  ┌─────────────────────────────┐
                  │ Diagnosis result, fault information │
                  │ database, and alarm for anomaly     │
                  └─────────────────────────────┘
```
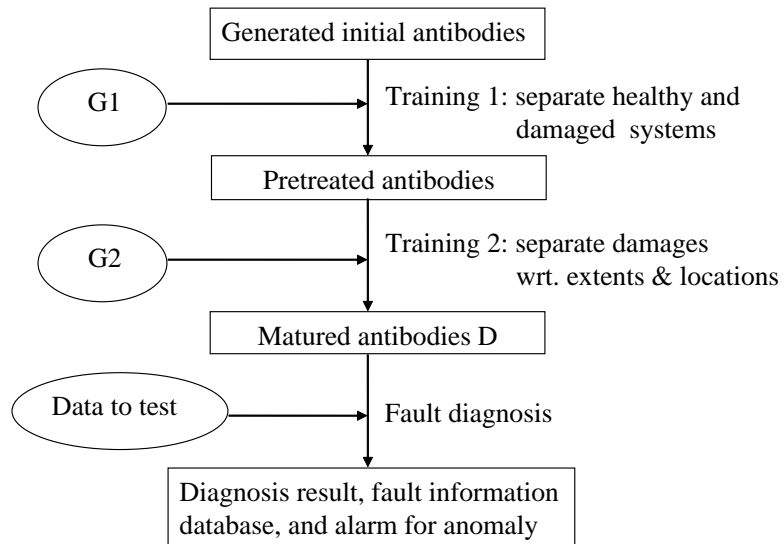
Fig.2.1 Main steps in training antibodies.

2.2 Selection of feature space

Structural health condition is characterized by a preselected feature space that consists of some indices sensitive to structural damage. In this study the system modal parameters including the natural frequencies, modal shape vectors, the modal masses, modal stiffness constants, and modal damping coefficient [61] are candidates for the feature space.

In this study, three different feature spaces are selected based on the natural frequencies and modal shapes of the structure, i.e. (I) the feature space of the first two natural frequencies, (II) the modal shape vector of the first mode, and (III) the modal shape vector of the second mode. Natural frequencies and modal shapes are inherent structural characteristics, independent of the initial conditions and the loading condition. They are sensitive to structural damage. Any structural stiffness loss due to damage may lead to change in their value. While the structural stiffness may not be easy directly measured, techniques such FFT are available to extract the natural frequencies and modal shapes either from vibration measurements or simulation data based on an appropriate structural model.

2.3 Identification of the feature space

To obtain the parameter values for the selected feature spaces, three main steps need to be taken. The first step is getting the vibration response data, which should be obtained by vibration measurements in a practical application. In this thesis, simulation data are used instead of measurement data due to insufficient experimental facilities. Thus the first step is model the structure and obtains the computer-simulated vibration response data. The second and the third steps are to extract the natural frequencies and the modal shape vectors from the simulation data, respectively.

2.3.1 Simulation of vibration response

2.3.1.1 Case study
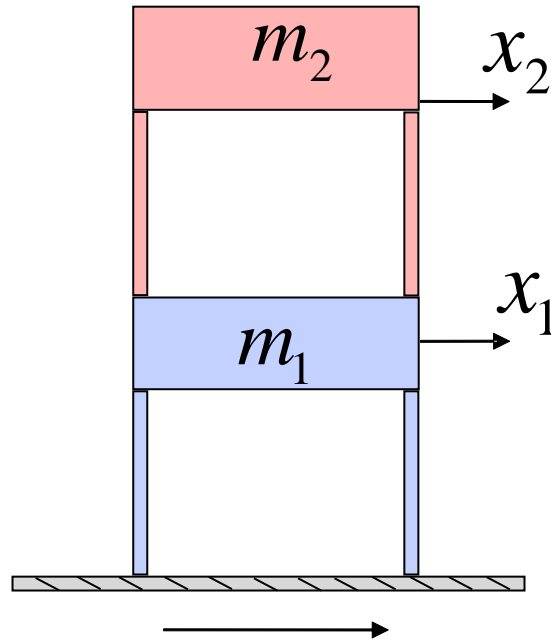
Fig.2.2 A sketch of a 2-storey building structure in the case study.

In this study, a 2-storey building with lumped floor masses and the lateral stiffness from columns is used as an example. Only small motion of floors in the horizontal direction is considered. The horizontal displacements x_1 and x_2 are relative to the ground. The feature spaces are extracted from three sources: (I) free vibration floor response data caused by a set of nonzero initial conditions; (II) the generalized eigenvalue problem associated with the mass and stiffness matrices from the theoretical model, and (III) forced vibration data under an earthquake ground motion.

2.3.1.2 Modeling

The 2-storey building can be simplified as a 2-DOF mass-spring-damper system as below:
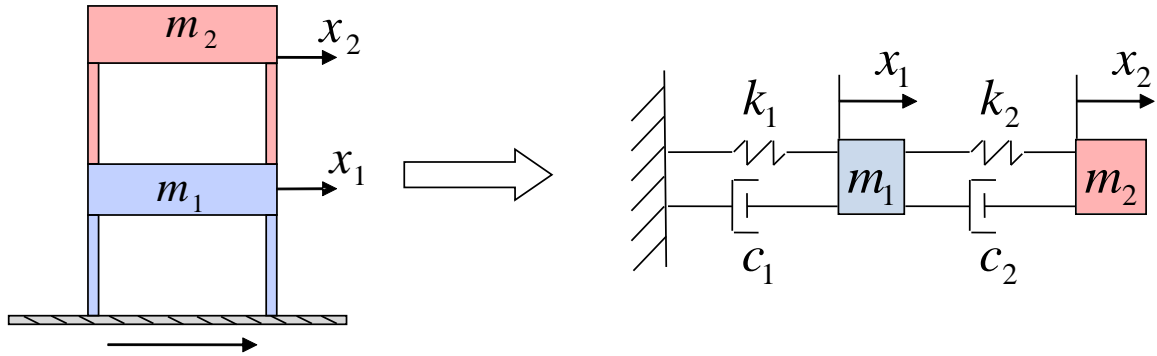
Fig.2.3   2-DOF mass-spring-damper system for the 2-story building structure.

In this system, m_1 and m_2 are the masses of the first floor and the second floor, respectively, k_1 and k_2 are the lateral stiffnesses of the first storey and the second storey. c_1 and c_2 are the damping coefficients to model the energy dissipation in the first and the second stories, respectively, f_1 and f_2 are the external forces applied on the first floor and the second floor in the horizontal direction, and x_1 and x_2 are the horizontal displacements of the first floor and the second floor relative to the ground.

Following the literature [62-64], the values of mass, stiffness, and damping are selected as:

$$m_1=m_2=m=2500 \ (N{\cdot}s^2/cm),$$

$$k_1=k_2=k=3{\times}10^6 \ (N/cm),$$

$$c_1=c_2=c=500 \ (N{\cdot}s/cm).$$

The IVP in matrix form is:

$$M\underline{\ddot{x}} + C\underline{\dot{x}} + K\underline{x} = \underline{F} \tag{2.8a}$$

$$\underline{x}(0) = \underline{x}_0 \tag{2.8b}$$

$$\underline{\dot{x}}(0) = \underline{v}_0 \tag{2.8c}$$

where

$$M = \begin{pmatrix} m_1 & 0 \\ 0 & m_2 \end{pmatrix} = \begin{pmatrix} m & 0 \\ 0 & m \end{pmatrix} \tag{2.8d}$$

$$K = \begin{pmatrix} k_1 + k_2 & -k_2 \\ -k_2 & k_2 \end{pmatrix} = \begin{pmatrix} 2k & -k \\ -k & k \end{pmatrix} \tag{2.8e}$$

$$C = \begin{pmatrix} c_1 + c_2 & -c_2 \\ -c_2 & c_2 \end{pmatrix} = \begin{pmatrix} 2c & -c \\ -c & c \end{pmatrix} \tag{2.8f}$$

If the system is in free vibration, the external forces are zero, thus at least one of the initial conditions values should not be zero.

$$F = \begin{pmatrix} f_1 \\ f_2 \end{pmatrix} = \begin{pmatrix} 0 \\ 0 \end{pmatrix} \tag{2.8g}$$

$$\underline{x}_0 = \begin{pmatrix} x_{01} \\ x_{02} \end{pmatrix}, \underline{v}_0 = \begin{pmatrix} v_{01} \\ v_{02} \end{pmatrix} \tag{2.8h}$$

If the system is in forced vibration in a seismic event, all of the initial conditions values are zero, while the external forces are non-zero inertial forces caused by the earthquake ground motion.

$$F = \begin{pmatrix} f_1 \\ f_2 \end{pmatrix} = \begin{pmatrix} -m_1 a_g \\ -m_2 a_g \end{pmatrix} \tag{2.8i}$$

$$\underline{x}_0 = \underline{0}, \underline{v}_0 = \underline{0} \tag{2.8j}$$

where a_g is the acceleration of the ground motion. Note that the horizontal displacements x1 and x2 are the motions relative to the ground in this case.

2.3.1.3 Calculation of the vibration response

There are several methods to calculate the vibration response for a linear multidegree-of-freedom (MDOF) systems including this 2-DOF mass-spring-damper system. Among them, the Runge–Kutta methods are an important family of implicit and explicit iterative methods for solving a first-order ordinary differential equations (ODE).[65] The fourth order Runge-Kutta method is commonly used, which is often referred to as "RK4", "classical Runge-Kutta method" or simply as "the Runge–Kutta method".

The RK4 for an IVP of the first-order system:

$$y' = f(t, y), y(t_0) = y_0 \qquad (2.9a)$$

is given by the following recursive equations starting from n=1:

$$y_{n+1} = y_n + \frac{1}{6}(k_1 + 2k_2 + 2k_3 + k_4) \qquad (2.9b)$$

$$t_{n+1} = t_n + h \qquad (2.9c)$$

where y_{n+1} is the RK4 approximation of $y(t_{n+1})$, h is the step length of time, and

$$k_1 = hf(t_n, y_n) \qquad (2.9d)$$

$$k_2 = hf(t_n + \frac{1}{2}h, y_n + \frac{1}{2}k_1) \qquad (2.9e)$$

$$k_3 = hf(t_n + \frac{1}{2}h, y_n + \frac{1}{2}k_2) \qquad (2.9f)$$

$$k_4 = hf(t_n + h, y_n + k_3) \qquad (2.9g)$$

Thus, the next value (y_{n+1}) is determined by the present value (y_n) plus the weighted

average of k_1, k_2, k_3, and k_4.

For each physical DOF, there are 2 associated unknown quantities: displacement and velocity, referred as the state variables. Thus the dimension of the state vector y for the 2DOF system in the study is 4, and their physical interpretation are, in a preset order, the displacement of the first floor (y1), the displacement of the second floor (y2), the velocity of the first floor (y3), and the velocity of the second floor (y4). Note that RK4 is used only for the first-order ODEs,. The ODE (2.8a) needs be converted to the ODE (2.9a) in the state space as follows:

$$\dot{y}1 = y3 \tag{2.10a}$$

$$\dot{y}2 = y4 \tag{2.10b}$$

$$\dot{y}3 = \frac{1}{m_1}\left(f_1 - c_1\dot{y}1 - k_1y1 - c_2\left(\dot{y}1 - \dot{y}2\right) - k_2(y1 - y2)\right) \tag{2.10c}$$

$$\dot{y}4 = \frac{1}{m_2}\left(f_2 - c_2\left(\dot{y}2 - \dot{y}1\right) - k_2(y2 - y1)\right) \tag{2.10d}$$

And the initial conditions in the IVP for RK4 (2.9a) are:

$$y_0 = \begin{bmatrix} x_{01} & x_{02} & v_{01} & v_{02} \end{bmatrix} \tag{2.10e}$$

After this step, displacements and velocities are obtained. Since acceleration is the first order derivative of velocity, the accelerations can be obtained by the calculation of velocities, that is, $\dot{y}3$ and $\dot{y}4$ in the above equations.

Fig.2.4 plots the acceleration of the ground motion recorded on September 14, 2010 recorder at Calexico area in Baja California, Mexico. The ground motion is used in this

study to generate the forced vibration response data in Case 3.
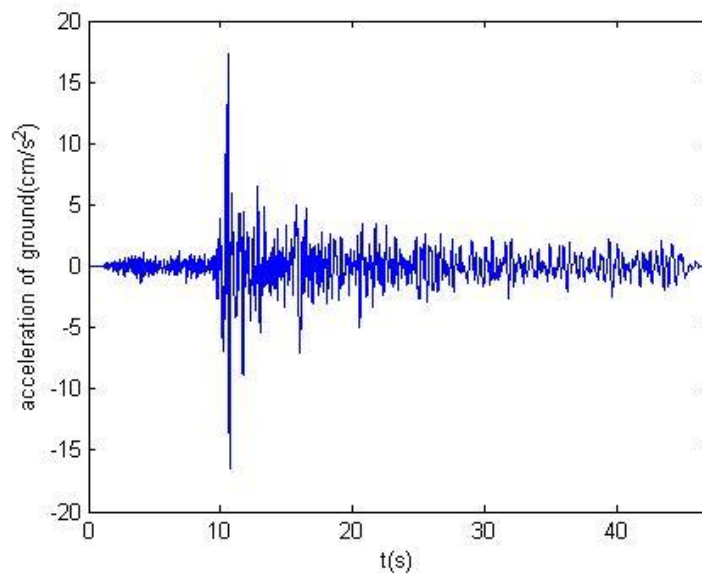
Fig.2.4 Earthquake on Sep 14, 2010. (Station Bonds Corner - Omlin Res). [66]

By using RK4, the vibration response is simulated. For example, a plot of the displacement for the 1st floor is given in Fig.2.5.
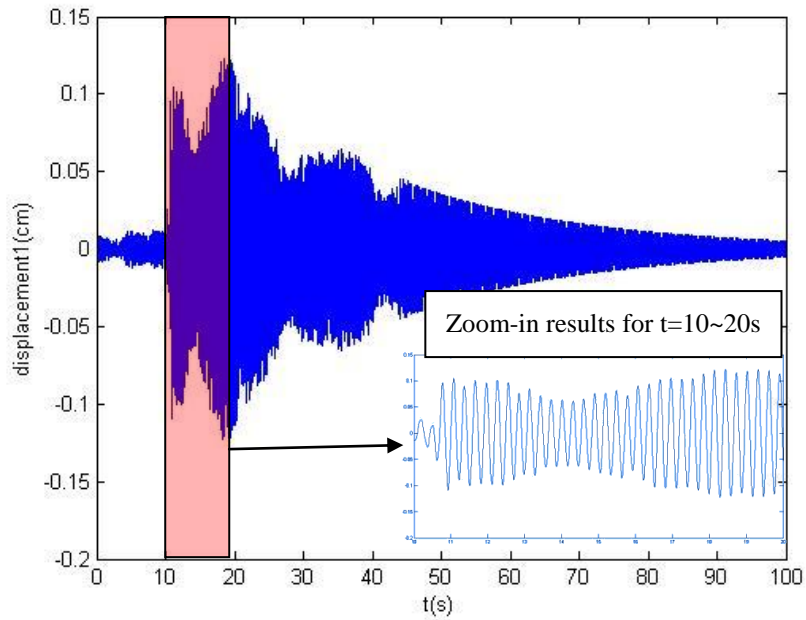
Fig.2.5 Displacement for the 1st floor under an earthquake ground motion.

2.3.2 Identification of the natural frequencies

After the first step, the displacements, velocities, and accelerations are obtained in time domain, which can transform to frequency domain information by using Fourier transform. Since the Fourier transform can transfer the time variable to the frequency variable, it reveals the inherent frequency characteristics of the signal and the relationship between time domain and frequency domain. The definition of Fourier transform is defined as:

$$F(\omega) = \mathcal{F}[f(t)] = \int_{-\infty}^{\infty} f(t)e^{-i\omega t}dt \qquad (2.11)$$

and the inverse of Fourier transform (IFFT) is given by:

$$f(t) = \mathcal{F}^{-1}[F(\omega)] = \frac{1}{2\pi}\int_{-\infty}^{\infty} F(\omega)e^{i\omega t}d\omega \qquad (2.12)$$

The natural frequencies can be identified by the abscissa values associated with some peaks in the Fourier response spectrum, i.e. the absolute value of the Fourier transform of a time response. For the spectrum from the free vibration data, all peaks are associated with the natural frequencies. However, for the spectrum from the forced vibration data, the peaks may associate with both the natural frequencies and dominant frequency content of the loading. Separation of the natural frequencies of the system from the dominant frequencies of the loading remains challenging.

Fourier transform is usually processed by computer in a discrete manner, i.e. discrete Fourier transform (DFT). In general, DFT requires great computational efforts. To

improve the computational efficiency Fast Fourier transform (FFT) employed in real

implementation such as the function "fft" in Matlab.

A frequency spectrum of the first-floor response under the given ground motion as shown

in Fig.2.4 is given in Fig.2.6 where two significant peaks can be observed. Note that the

spectrum is from the seismic response data and the peaks there are generally associated

with both system and the loading. However, the earthquake ground motion in this is a

white-noise like signal with a wide frequency range. Therefore, the two dominant peaks

are actually represents two natural frequencies of this 2-DOF mass-spring-damper system

and the first peak corresponds to mode 1 while the second peak corresponds to mode 2.
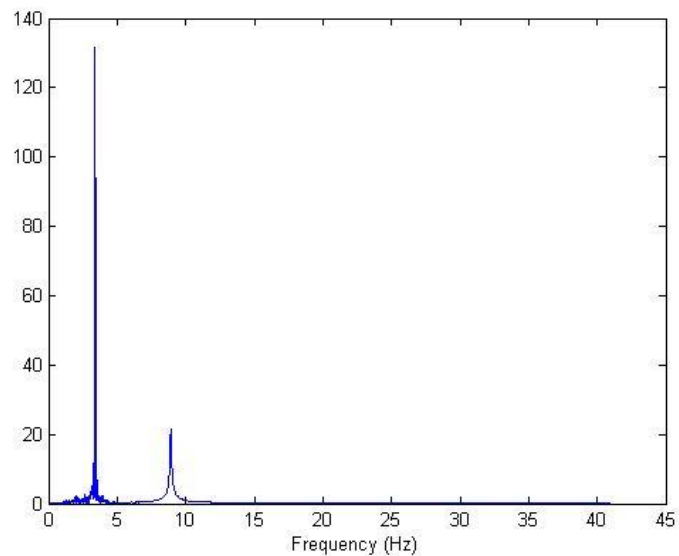
Fig.2.6 Fourier response spectrum of the 1st floor response under the given earthquake
ground motion.

2.3.3 Extract modal shape information

By the principle of modal analysis the structural response can be viewed as superposition of two modal responses, each associated with a distinct modal shape vector. For the purpose of extracting the modal shapes contribution to the total response from two modes need to be separated. This can be done in a two-step procedure.

Using the Fourier transform of the two floors we may first determine the position of the dominant peaks in the response spectra, which would associate with the system natural frequencies. We may then filter the response in the frequency domain in the vicinity of each peak and perform the inverse Fourier transform for the filtered frequency domain signal, which leads to the modal response associated with the specific natural frequency. Using the modal responses of both floors for each mode, we may determine the associated modal shape vector for each mode. For mode 1, assume the amplitude of the filtered modal response of the first floor is $x_1^{(1)}$, and that of the second floor $x_2^{(1)}$. Note that at each time point, the ratio of $x_1^{(1)}/x_2^{(1)}$ should be in fact constant, thus the vector $(x_1^{(1)}, x_2^{(1)}) \propto \underline{X}^{(1)}$, the mode shape vector of the first mentioned in Section 1.2. Similarly, for mode 2, $(x_1^{(2)}, x_2^{(2)}) \propto \underline{X}^{(2)}$. In other words, the ratios can uniquely represent the characteristic of the modal shapes.

In the filtering process to pick out the peak for each mode in the plot of the frequency

domain, the Gauss window function in Matlab is employed. In signal processing, a window function is a mathematical function that is zero-valued outside of some chosen interval. We may place the Gauss window in the vicinity of each peak and filter the signal in the frequency domain by the window function. In Matlab, the function "w=gausswin(N, α)", as in Eq. (2.13) returns an N-point Gaussian window in the column vector w, where α is proportional to reciprocal of the standard deviation.

$$w(n) = e^{-\frac{1}{2}(\alpha\frac{n}{N/2})^2} \tag{2.13}$$

where $-\frac{N}{2} \leq n \leq \frac{N}{2}$, α is inversely proportional to the standard deviation of a Gaussian distribution. The Gauss window, as shown in Fig.2.7, should hold the information at the middle of the interval and decrease the amplitude to zero smoothly to the both sides of the interval. By carefully selecting the α-value, or alternatively, the standard deviation, the Gauss window will appropriately filter the frequency-domain signal in the required frequency range such that the extracted modal responses would not be too much distorted.
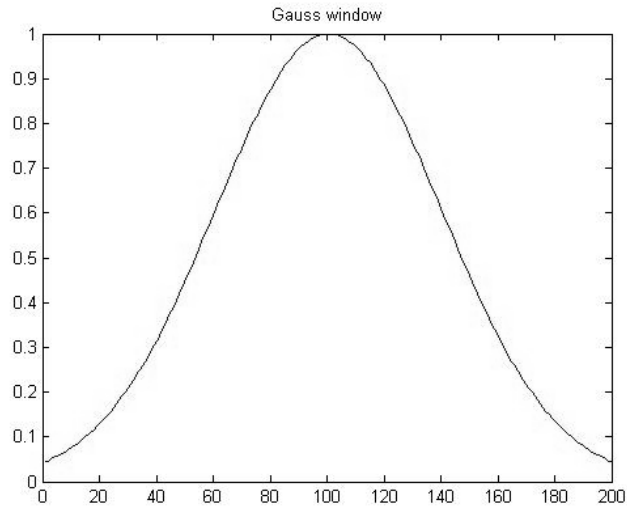
Fig.2.7 A Gauss window (n=200, α=2.5 in Eq(2.13)).

Since the external force of this 2-DOF mass-spring-damper system is from the earthquake, its frequency content will be complex. Thus, in the plot of the frequency domain, the wave crest for each mode will not be smooth. The little wave near the peak will disturb the result after IFFT. To weaken the influence of the little wave, the plot needs a filter before picking out the modes. The moving average filter is selected to make sure that the data is symmetric after filtering. Though the modal shape vectors can also be extracted from the velocity and acceleration responses in a similar way, the results from the displacement responses provided best match as compared to the theoretical results by the eigenvalue problem and ,therefore, only the latter is presented in the thesis.

2.4 AIS algorithm

There are three main components of the AIS algorithm for SHM: determine the antigens, trainings for the antibodies, and fault diagnosis by using the matured antibodies, as indicated by the blocks with different colors shown in Fig.2.8.
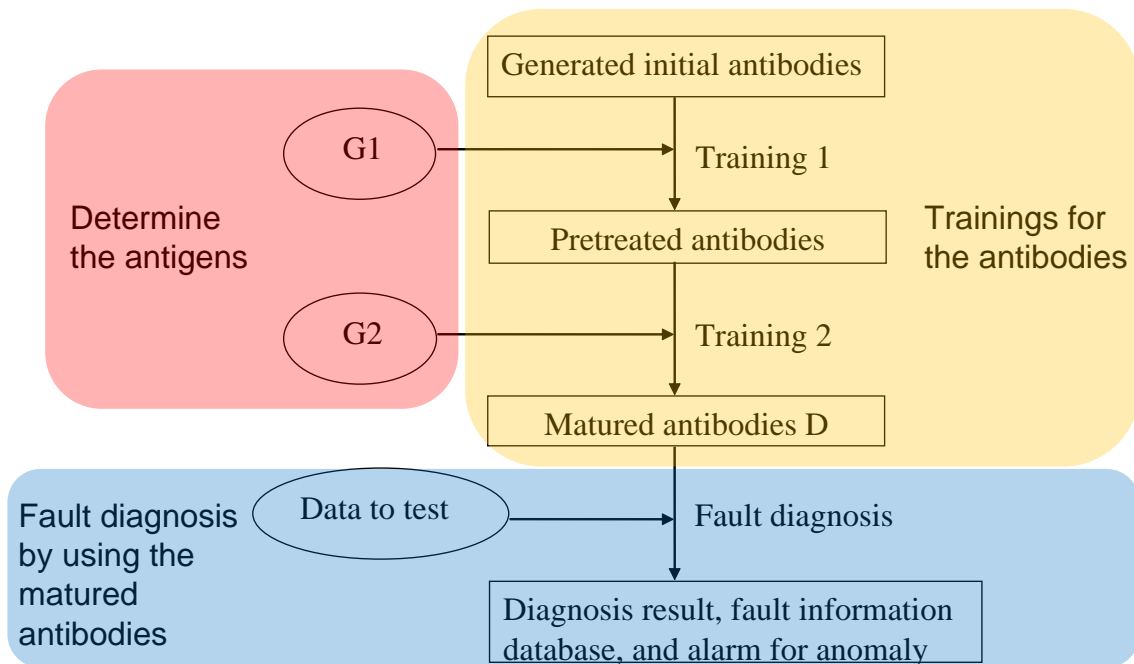
Fig.2.8 The three main components of the AIS algorithm.

2.4.1 Determine the antigens and antibodies

The antigens and antibodies will be determined by natural frequencies and mode shapes for each mode. First of all, vector expressions need to be set. If frequencies are used to do the AIS fault diagnosis, the N-dimensional state vector which mentioned in the Section 2.1 has a dimension of 2, the first component is the frequency of mode 1, and the second is that of mode 2. The vector expression is:

$$V=(\text{frequency 1, frequency 2}) \tag{2.14}$$

If modal shape 1 is used as the feature space, the vector expression is:

$$V=(x_1^{(1)}/x_2^{(1)}, 1) \tag{2.15}$$

If modal shape 2 is used as the feature space, the vector expression is:

$$V=(x_1^{(2)}/x_2^{(2)}, 1) \tag{2.16}$$

When the 2-DOF mass-spring-damper system is in the normal condition, there is only one state vector, this original state vector can be used to generate a set of state vectors in the feature space by a cloning process as a set of the first kind of antigens, named as G_1, to stand for possible normal conditions. In the Matlab program, it is implemented by generating a set of random vectors around the original state vector in a certain range. This "certain range" depends on the distance between the first kind of antigens and the second kind of antigens which will show later.

When the system is in the abnormal condition, the stiffness k_1 or k_2 will change. In other

words, k_1 or k_2 will decrease when the 2-storey building is damaged. To determine the damage location and extent, set the k_1 or k_2 to the N-tenth of k, respectively, where N=1, 2, …, 9. Therefore, there are 18 cases of damage in total listed in Table 2 that, correspond to 18 antigens of the second kind, represented by 18 state vectors in G_2. It is assumed that two springs are not damaged at the same time, partially for simplicity and partially because of the reality since there is only very small chance the event would occur.

Table 2 The 18 cases of damage patterns

Case number		Extent								
		10%	20%	30%	40%	50%	60%	70%	80%	90%
Location	k_1 loses only	1	2	3	4	5	6	7	8	9
	k_2 loses only	10	11	12	13	14	15	16	17	18

Once the two kinds of antigens are obtained, and the "distance" between them can be determined. The "certain range" was selected to be less than the distance between the original state vector of G_1 and the state vector of case 1 and case 10 in G_2. Since the state vectors are normalized so that all variables take values in the interval [0, 1], and the random variables are also in the interval [0, 1], each vector of G_1 is the sum of the original state vector and a thousandth of a random state vector in my program for the example system.

2.4.2 Trainings for the antibodies

To get the matured antibodies, a huge number of initial antibodies should be generated randomly, which are shown in Fig.2.9 and the stars, which are grouped in the circle, are the first kind of antigens G_1. These set of random state vectors will be trained twice before becoming matured antibodies. This "huge number" must be big enough so that the random state vectors can cover all the situations including normal and abnormal conditions. After a series of trials, the "huge number" is determined as a number greater than 1000.
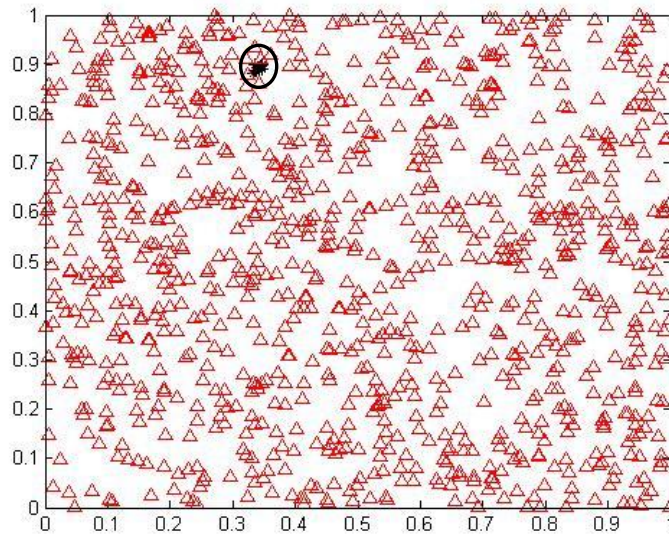
Fig.2.9 Initial antibodies (triangles) in the feature space

When the initial antibodies are prepared, the training starts with two major steps. The first is clearing away the initial antibodies which are close to the first kind of antigens defined in G_1 and generate new random antibodies to keep the total number of antibodies as the constant until none of the antibody is close to G_1. The second is clearing away the

antibodies which are far away from the second kind of antigens G_2 and letting the other vectors move closer to them. The criterion of "close to" and "far away" is based on the affinity between the antigens and antibodies. The value of affinity depends on the distance between the first kind of antigens and the second kind of antigens. In other words, the critical affinity of Training 1 is the affinity which will let an antibody that:

I   outside the area of the first kind of antigens G_1,

II   between the first kind of antigens and the antigens of the second kind which are near

to G_1 (the Case 1 for k_1 loses 10% and the Case 10 for k_2 loses 10%).

Since the first kind of antigens is very close to the Case 1 and Case 10 in the second kind of antigens G_2, the critical affinity will near 1. After a series of test, the best value of this affinity is 0.97, and the antibodies after the first training are shown in Fig.2.10.
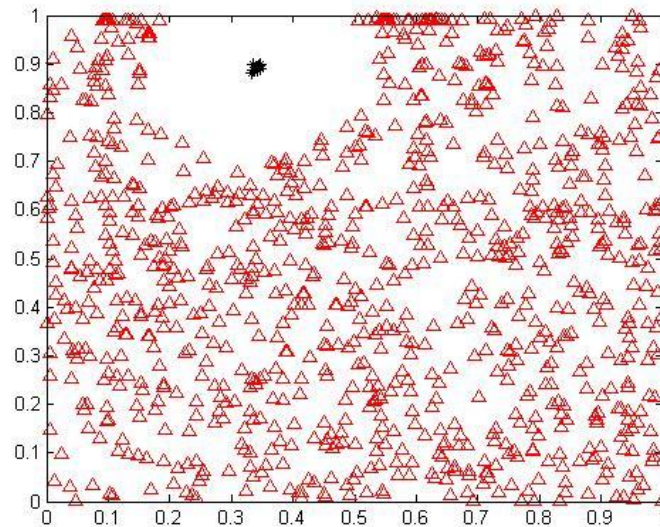
Fig.2.10 After training 1, the antibodies (triangles) are separated from the first kind of antigens G_1(stars).

For Training 2, the critical affinity must make the vectors move closer to each second

antigen of G_2 obviously. Like Training 1, it will near 1. The trials suggests a value of 0.96, and the result of the matured antibodies using natural frequency as feature spaces using the seismic response data is in Fig.2.11.
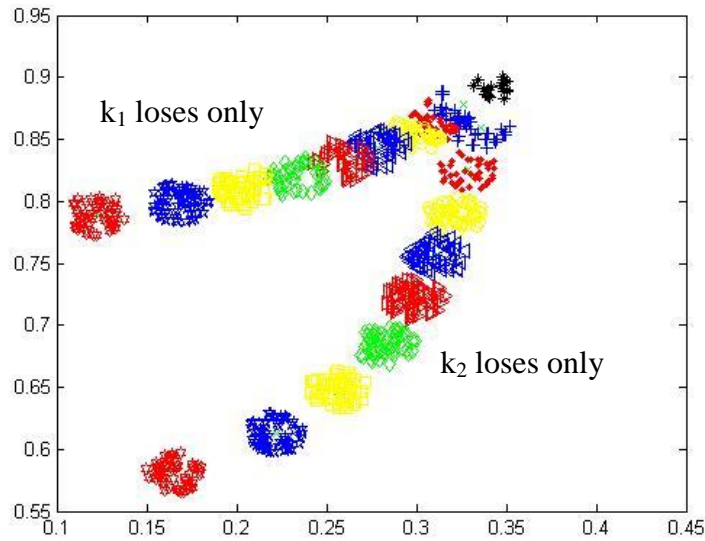
Fig.2.11 The antibodies after training 2 for 18 cases of damage, differentiated by colors and shapes.

In the above picture, plus-mark stand for 10% loss of k_1 or k_2; point stand for 20% loss of k_1 or k_2; circle stand for 30% loss of k_1 or k_2; triangle (left) stand for 40% loss of k_1 or k_2; triangle (right) stand for 50% loss of k_1 or k_2; diamond stand for 60% loss of k_1 or k_2; square stand for 70% loss of k_1 or k_2; pentagram stand for 80% loss of k_1 or k_2; hexagram stand for 90% loss of k_1 or k_2. Stars are the first kind of antigens G_1, and the x-marks are the second kind of antigens G_2 which are not clear in the plot for they are nearly buried by the antibodies.

2.4.3 Fault diagnosis by using the matured antibodies

After these two trainings, the antibodies are matured and ready to process the fault diagnosis. The matured antibodies D are the database or the data information system for the 18 cases of damage showing the location and extent of damage. The databases for different case studies using different feature spaces will be detailed later in the in the part of Results. Given new response data from the realistic measurements we can extract the modal information including the natural frequencies and the modal shapes and draw structural health condition by matching them with the matured antibodies. For example, if the state vector in the feature space represents the natural frequencies and if the newly extracted frequencies in the area of the first kind of antigens G_1, the building is healthy, or otherwise it is damaged. Note that there are two branches with different colors in the matured antibodies shown in the feature space which correspond different cases of damage as defined in Table 2. Therefore, the trained database can also be used to determine the damage location and the damage severity. For example, if the newly extracted state vector matches Case 5 in G_2, the building is damaged at the first storey and the extent of damage is about 50% stiffness loss of k_1.

In the similar way, the matured antibodies trained by the feature space of the modal shapes can also be used to locate the damage and assess the damage severity. Note that the state vector for modal shapes needs to be normalized first to make sure that all

components are in the interval [0, 1] in the process of generating G_1, the first kind of antigens and G_2, the second kind of antigens corresponding to the 18 cases of patters. Given a set of new response data, one can extract the modal shapes based on the ratio, i.e. $x_1^{(1)}/x_2^{(1)}$ for modal shape 1 and $x_1^{(2)}/x_2^{(2)}$ for modal shape 2. The location of the state vector corresponding to this ratio will show the case of damage, and in turn, the damage location and the damage severity.

Figures 2.12 through 2.14 illustrate an example of the testing case where k_1 loses 45%. Solving the eigenvalue problem, the natural frequencies are found to be 2.6890Hz and 8.3833Hz for two modes, respectively, and the modal matrix Φ is:

$$\Phi = \begin{bmatrix} -0.0121 & -0.0159 \\ -0.0159 & 0.0121 \end{bmatrix}$$

After normalization, the state vectors of this testing case are (0.2689, 0.8383) in the feature space of natural frequencies, (0.6062, 0.7953) in the feature space of modal shape 1, and (-0.7953, 0.6062) in the feature space of modal shape 2. Consistent results are observed in all three figures regarding the damage location and the damage extent, as compared to the theoretical results.
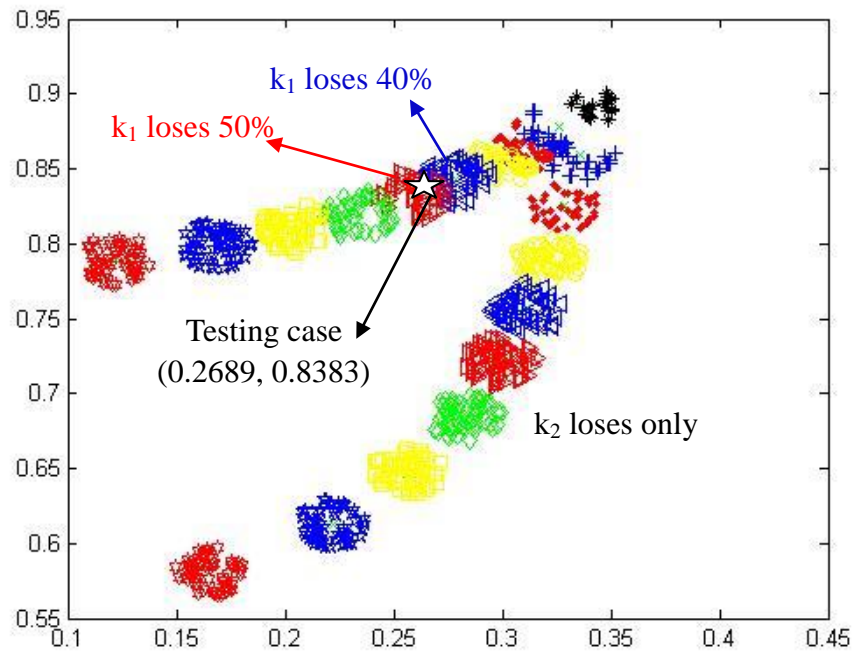
Fig.2.12 Damage location and extent identified by the matured antibodies in the feature space of the natural frequencies.
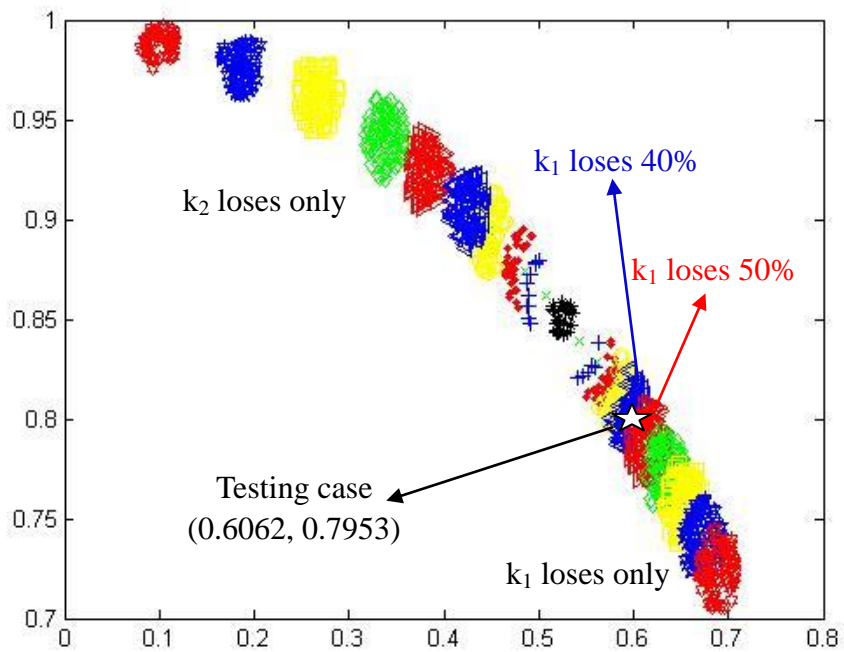
Fig.2.13 Damage location and extent identified by the matured antibodies in the feature space of the modal shape 1.
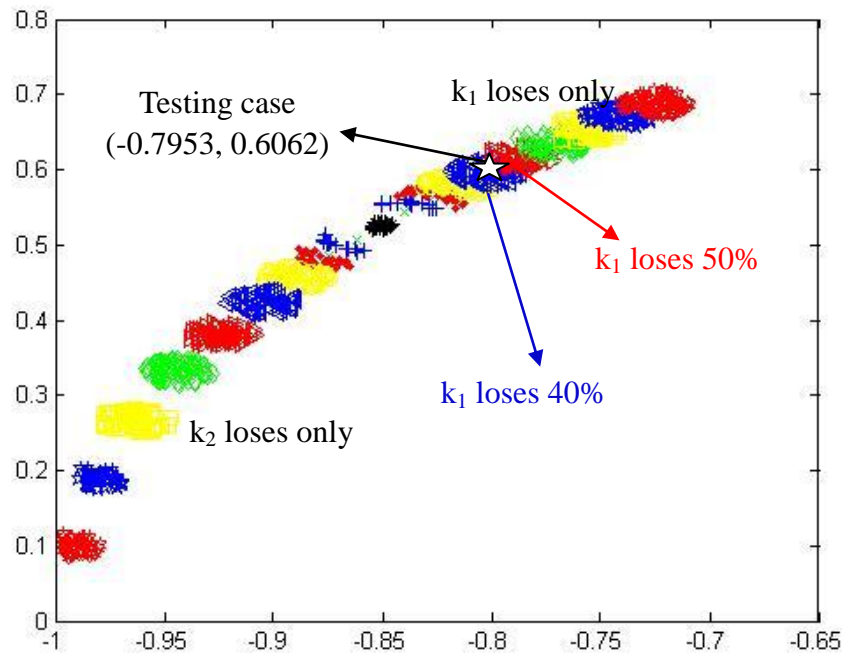
Fig.2.14 Damage location and extent identified by the matured antibodies in the feature space of the modal shape 2.

3 Results

This part presents about the results for fault diagnosis of a 2-storey building by using the AIS algorithm. The 2-storey building is simplified as a 2-DOF mass-spring-damper system as below:
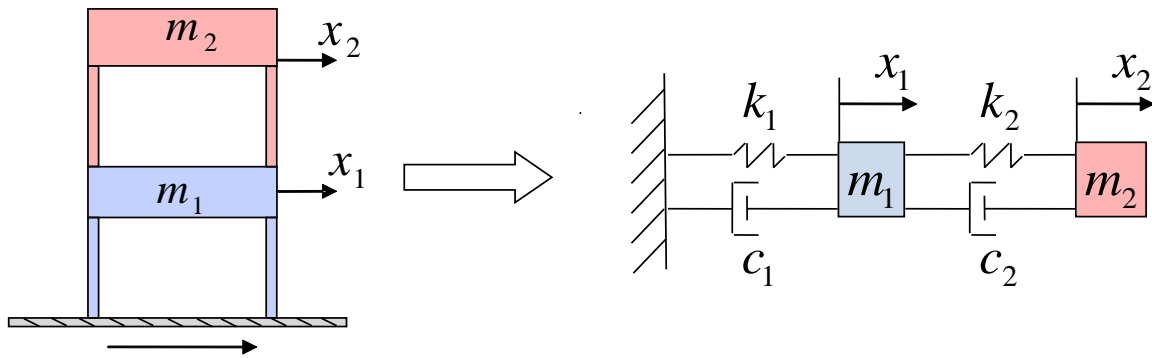
Fig.3.0 2-DOF mass-spring-damper system.

In this system, $m_1=m_2=2500$ (N·s^2/cm), $k_1=k_2=3\times10^6$ (N/cm), $c_1=c_2=500$ (N·s/cm). There are two studies: free vibration caused by nonzero initial conditions and forced vibration under seismic excitation. When the system is in free vibration, the external excitation is the inertial force from an earthquake ground motion. The earthquake data [66] is from the United States Geological Survey (USGS) recorded on September 14, 2010 for Calexico area earthquake in Baja California, Mexico. The testing case is for the damage caused by 45% stiffness loss of k_1 only. The vectors are: $v=(0.2689, 0.8383)$ for the feature space of natural frequencies, $v=(0.6062, 0.7953)$ for the feature space of modal shape 1, and $v=(-0.7093, 0.6062)$ for the feature space of modal shape 2 as calculated by the associated eigenvalue problem.

To apply the AIS algorithm, antibodies and antigens are introduced. The antibodies are the database or the information system to be trained for the AIS fault diagnosis, while the antigens are the known structural health condition used in the training process. Three different feature spaces are used in this study: the natural frequencies, the modal shape 1, and the modal shape 2. Two different kinds of antigens are used: G_1 for the healthy structure and G_2 for 18 cases of damage patterns. A large number of the initial antibodies are generated by computer as random vectors in the pre-selected feature space. These antibodies are then trained with the antigens, and the matured antibodies become a useful information system for the AIS-based fault diagnosis.

3.1 Study 1: Free-vibration data

3.1.1 Using the natural frequencies as the feature space

Natural frequencies can be extracted from the Fourier response spectrum of the response, as shown, for example, a plot for the response spectrum of a free-vibration response of the healthy system in Fig.3.1.1.1. There are two peaks in the plot, the left one corresponds to the natural frequency of the first mode and the right one corresponds to that of the second mode. When the system is under normal condition, the natural frequencies are 3.41 Hz and 8.91 Hz.
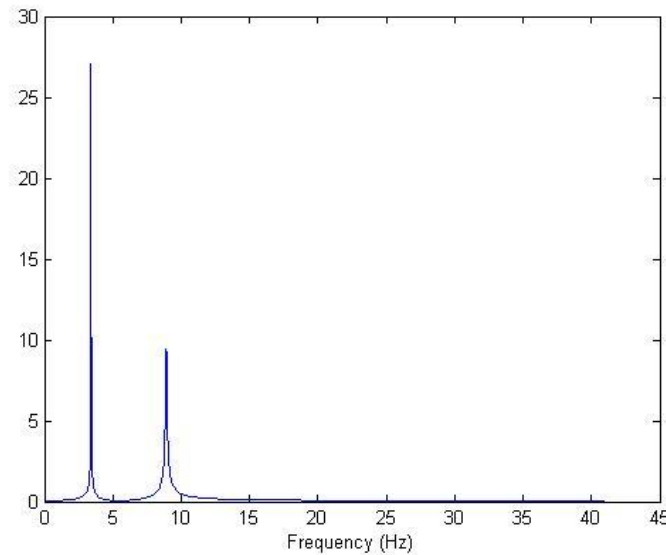
Fig.3.1.1.1 The Fourier response spectrum of a simulated free vibration response of the healthy structure.

When the building is damaged, the shape of frequency response spectrum of the free-vibration response is similar to the plot above, but the values of peaks are different, and the position of the peaks are shifted to the left, i.e. the natural frequencies are smaller

than those of the healthy structure. Fig.3.1.1.2 and Fig.3.1.1.3 show the variation of the

natural frequencies corresponding to different damage levels:
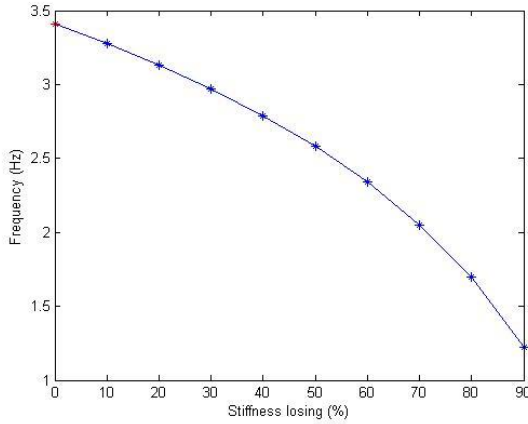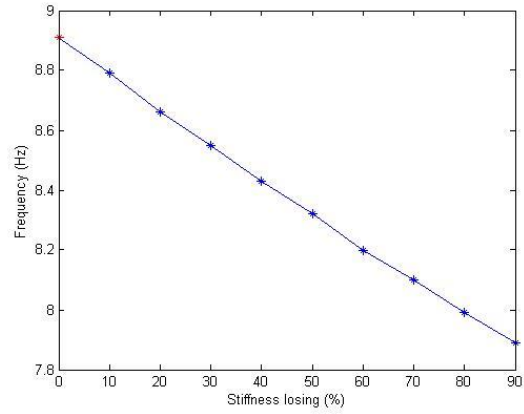
(a)   (b)

Fig.3.1.1.2 Frequency is decreasing with the stiffness loss of k_1.
(a) is for mode 1 and (b) is for mode 2
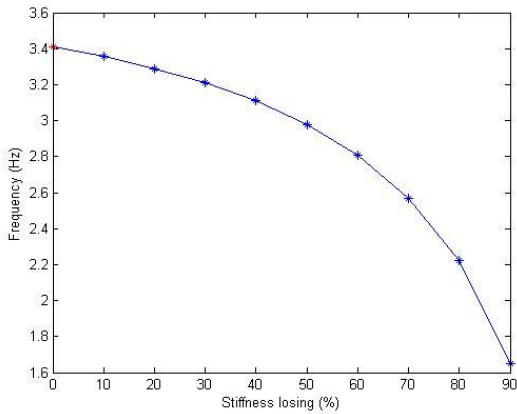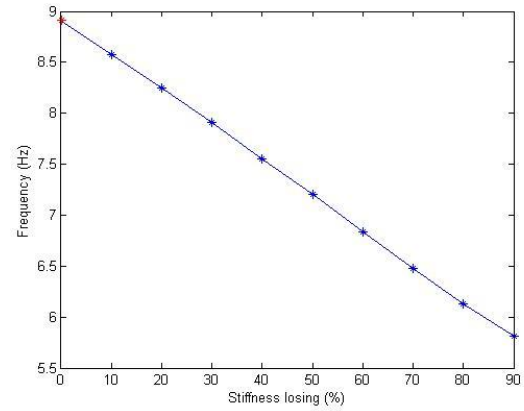
(a)   (b)

Fig.3.1.1.3 Frequency is decreasing with the stiffness loss of k_2.
(a) is for mode 1 and (b) is for mode 2

Since the natural frequencies are 3.41 Hz and 8.91 Hz for the healthy structure, the state

vector for generating the first kind of antigens G_1 is (3.41, 8.91) or (0.341, 0.891) after

normalization. The second kind of antigens G_2 is a set of the state vectors normalized

from the values in Fig.3.1.1.2 and Fig.3.1.1.3. After the trainings, the matured antibodies

in the feature space of the natural frequencies are shown in Fig.3.1.1.4 and Fig.3.1.1.5,

one for k_1-loss only and the other for k_2-loss only.
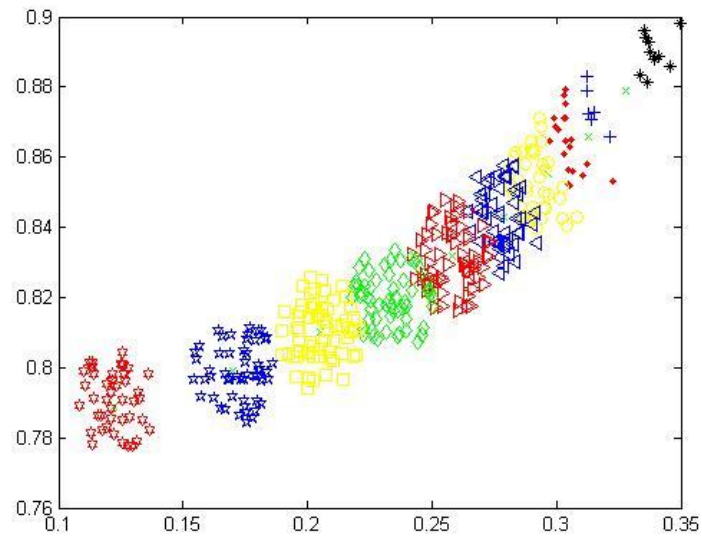
Fig.3.1.1.4 Matured antibodies in the feature space of natural frequencies using the
free-vibration data (k_1-loss only).

The stars are the first kind of antigens G_1, and the x-marks are the second kind of

antigens G_2 which are not clear in the plot for they are nearly buried by the antibodies.

The other points in this figure are the matured antibodies. The plus-marks which are near

to the stars correspond to the condition when the stiffness k_1 loses by only 10%, while the

hexagrams which are far from the stars correspond to the condition when the stiffness k_1

loses by 90%.

Fig.3.1.1.5 Matured antibodies in the feature space of natural frequencies using the free-vibration data (k_2-loss only).

(0.2689, 0.8383)

Fig.3.1.1.6 Comparison of the matured antibodies in the feature space of natural frequencies using free-vibration data for k_1-loss and k_2-loss.

For the purpose of comparison, the results are plotted in one figure as shown in Fig.3.1.1.6. It is observed that the matured antibodies are well separated as two lines: the

upper line is for k_1-loss only and the lower line is for k_2-loss only. To test the matured antibodies for fault diagnosis, a case of 45% k_1-loss is considered and the result is mark as in the figure by a white star that is located roughly between two groups of antibodies corresponding the 40% k_1-loss and 50% k_1-loss, respectively. It may conclude in this case that the trained antibody information system can be used for structural health monitoring. It can tell from the results if the structure is damaged and, if damage occurred, the damage location, and the damage severity. It is also observed that two lines representing the stiffness loss at different locations are well separated if the stiffness loss is more than 50%. For the stiffness loss less than 20% two parts of antibodies merges and the two lines become non-separable by naked eyes. The situation may be improved if the matured antibodies in the feature space of the modal shapes are used as shown by the results in Section 3.1.2

3.1.2 Using a modal shape as the feature space

To extract the modal shapes from the response data, the signals need to be filtered in the frequency domain. In this study the MATLAB function for the Gaussian window, i,e, "gausswin(N, α)" in used for each mode. Parameters N and α specify the width and the sharpness of the window, respectively. The frequency range of Fig.3.1.1.1 is 40.95 Hz with 4096 points. Therefore, the first peak at 3.41 Hz, i. e. the first natural frequency is at about the 341th point in the plot. In the study, the Gauss window is placed in the vicibity of the first peak from the 241th point to the 441th point on the plot, corresponding to N=200 in the Matlab function "gausswin(N, α)". Consider with the theoretical value which will be mentioned in Section 3.2, the best choice of "α" is between [25, 35]. Using gausswin(200,30) to filter the signal in the frequency domain, the ratio $x_1^{(1)}/x_2^{(1)}$ for modal shape 1 can be determined.

The ratio $x_1^{(1)}/x_2^{(1)}$ for modal shape 1 for the healthy system is 0.6236 from free-vibration data. The variation of the ratios due to the stiffness loss is shown in Fig.3.1.2.1.
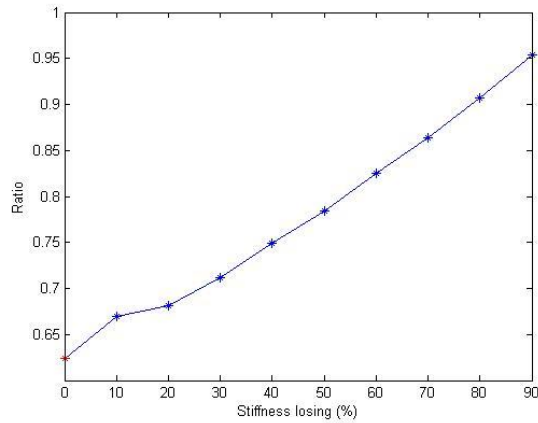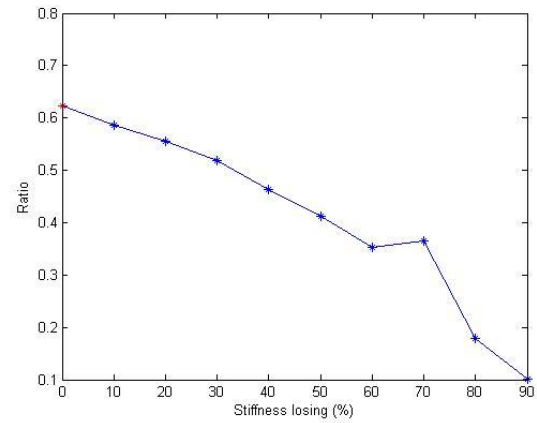
Fig.3.1.2.1 Variation of the modal shape ratio for modal shape 1 due to the stiffness loss extracted from the free vibration data.
(a) is for k_1-loss and (b) is for k_2-loss

The state vector for the antibodies in the feature space of mode 1 can be generated based on the ratio. The first kind of antigens G_1 is generated as (0.6236,1) original or (0.5291, 0.8485) after normalization. The second kind of antigens G_2 are generated as a large size of group of the normalized state vectors in the feature space as shown in Fig.3.1.2.1. After the trainings, the matured antibodies are shown in Figures 3.1.2.2 through 3.1.2.4.
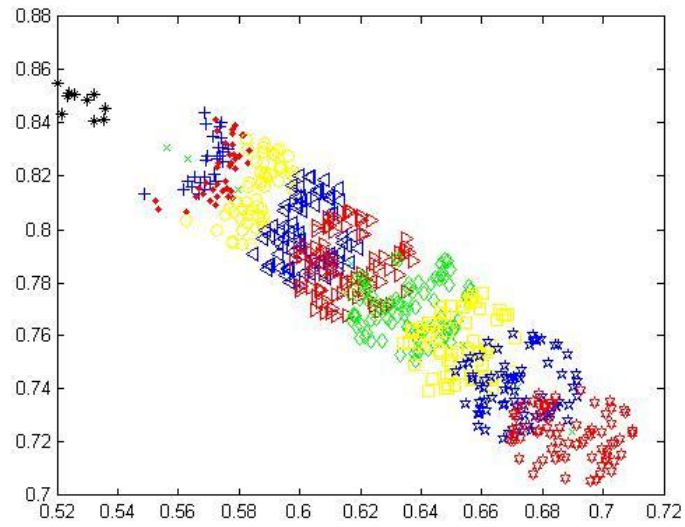
Fig.3.1.2.2 Matured antibodies in the feature space of modal shape 1 using free-vibration data (k_1-loss only).
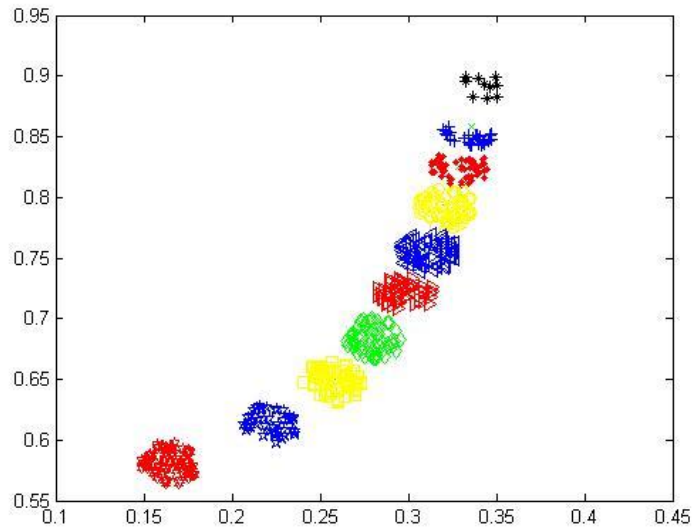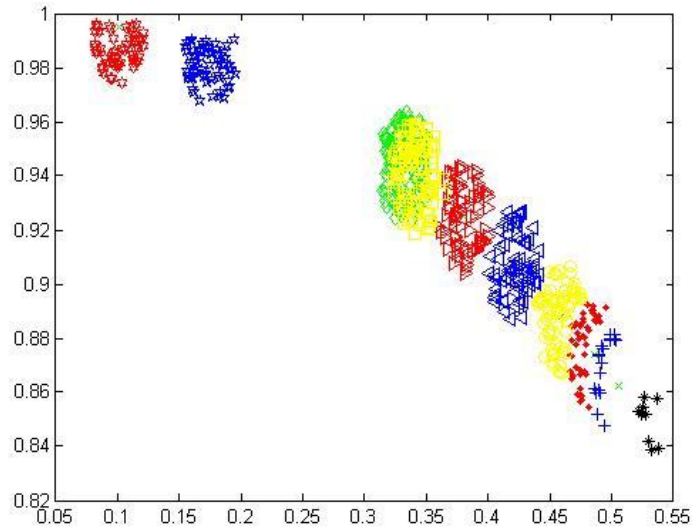

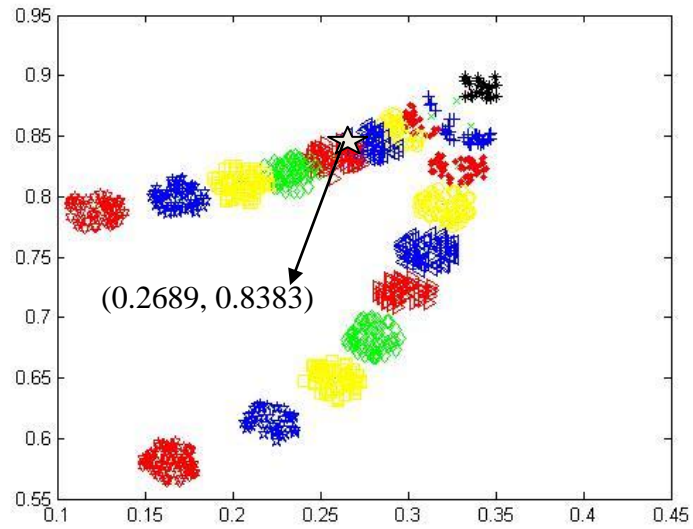Fig.3.1.2.3 Matured antibodies in the feature space of modal shape 1 using free-vibration data (k_2-loss only).
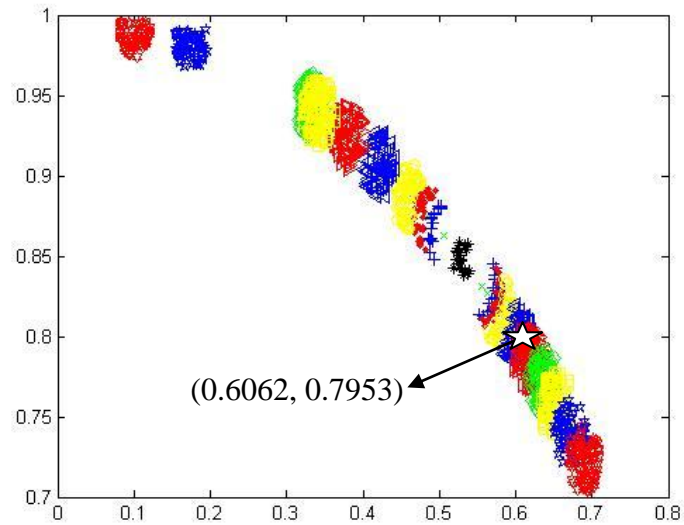
Fig.3.1.2.4 Comparison of the matured antibodies in the feature space of modal shape 1 using free-vibration data for k_1-loss and k_2-loss.

In Fig.3.1.2.4, the lower line is for k_1 and the upper line is for k_2 are clearly separated for all the range of stiffness loss. The testing case of 45% k_1-loss is shown on the plot by the white star purpose of fault diagnosis. Again, the matured antibodies or the trained information system in the feature space of modal shape 1 can be effectively applied for SHM. In contrast to the results in the feature space of natural frequencies, the scheme works better for a small stiffness loss since the lines of the antibodies for stiffness loss in different locations run the opposite directions: one is up and the other is down.

Similar results are obtained if using the feature space of modal shape 2. The ratio $x_1^{(2)}/x_2^{(2)}$ for modal shape 2 is analytically determined as -1.6180 for the healthy structure. Variation of the ratio due to the stiffness loss is shown in Fig.3.1.2.5.
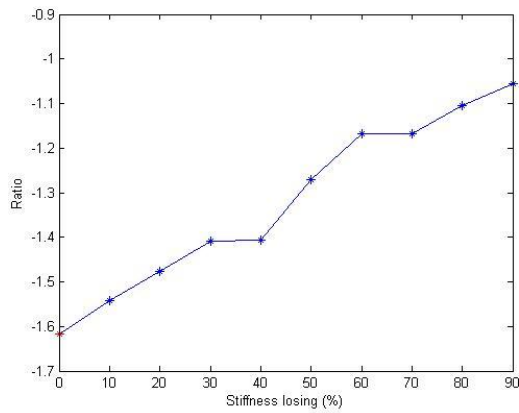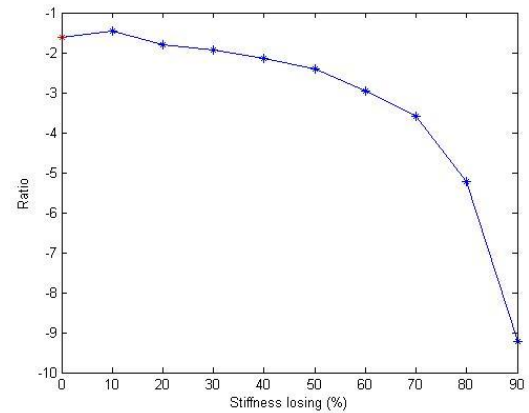
Fig.3.1.2.5 Variation of the modal shape ratio for modal shape 2 due to the stiffness loss
extracted from the free vibration data.
(a) is for k_1-loss and (b) is for k_2-loss

The state vector for antibodies in the feature space of modal shape 2 can be determined based on the ratio $x_1^{(2)}/x_2^{(2)}$. The first kind of antigens G_1 is generated as (-1.6180, 1) originally or (-0.8506, 0.5257) after normalization. The second kind of antigens G_2 are generated as a large size of a group of the normalized state vectors I the feature space as shown in Fig.3.1.2.5. After the trainings, the matured antibodies are shown in Figures 3.1.2.6 through 3.1.2.8.
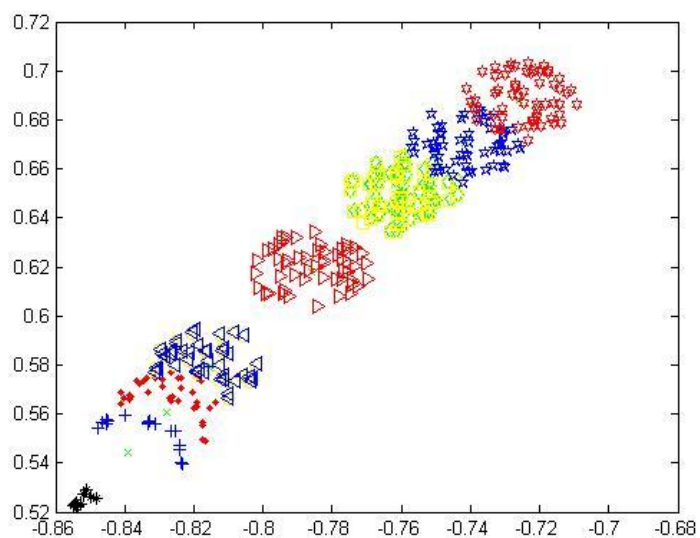
Fig.3.1.2.6 Matured antibodies in the feature space of modal shape 2 using free-vibration data (k_1-loss only).
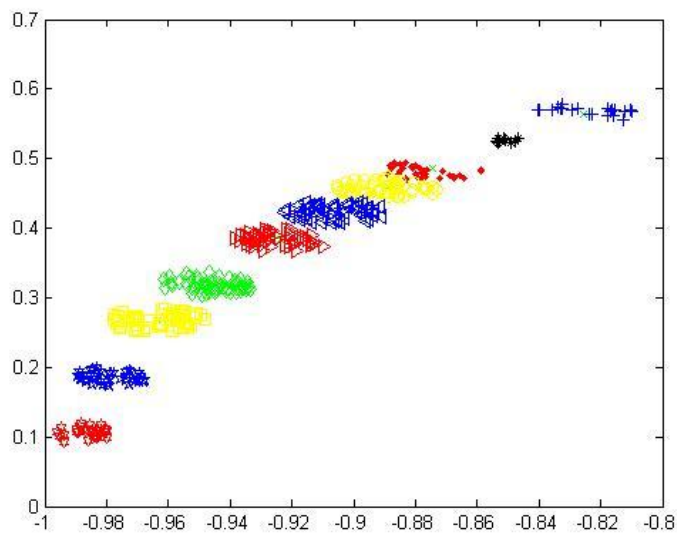
Fig.3.1.2.7 Matured antibodies in the feature space of modal shape 2 using free-vibration data (k_2-loss only).
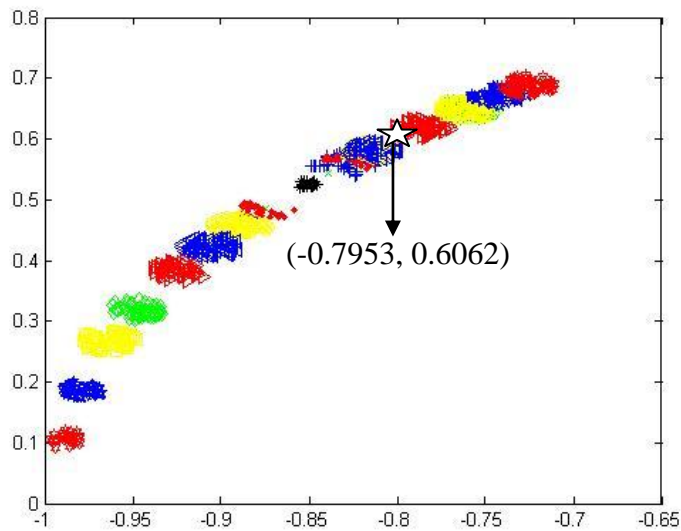
Fig.3.1.2.8 Comparison of the matured antibodies in the feature space of modal shape 2 using free-vibration data for k_1-loss and k_2-loss.

In Fig.3.1.2.8, the upper line is for k_1–loss and the lower line is for k_2-loss. The white star is the result for the testing case of 45% k_1-loss for application of the information system for SHM. Potentials of the AIS scheme are illustrated again by the results for damage detection, damage location, and damage assessment. Similarly to the results using the feature space of the modal shape 2, two lines run in opposite directions, which provide a merit of locating damage for a small stiffness loss.

3.2 Study 2: Data from eigen-solution

To check the results in Section 3.1, eigenvalue method should be used, the results from which are theoretical values. The database obtained by theoretical values can give rough estimate when the measurement data are not sufficient. Using the Matlab function "eig", the natural frequencies (in rad/s) and modal matrix Φ are obtained. The natural frequencies need transform, so that the unit changes to Hz, which is the same as the unit of the plot in frequency domain. The j-th column of the modal matrix Φ, which is shown in Eq (3.1), is the modal shape vector $\underline{X}^{(j)}$ for mode j.

$$\Phi=[\underline{X}^{(1)} \ \underline{X}^{(2)}]=\begin{bmatrix} x_1^{(1)} & x_1^{(2)} \\ x_2^{(1)} & x_2^{(2)} \end{bmatrix} \tag{3.1}$$

Thus the ratio $x_1^{(1)}/x_2^{(1)}$ for modal shape 1 and the ratio $x_1^{(2)}/x_2^{(2)}$ for modal shape 2 can be obtained. When the building is under the normal condition, the natural frequencies for the both modes are 3.4074 Hz and 8.9207 Hz, and the ratio $x_1^{(1)}/x_2^{(1)}$ for modal shape 1 is 0.6180, the ratio $x_1^{(2)}/x_2^{(2)}$ for modal shape 2 is -1.6190.

3.2.1 Using the natural frequencies as the feature space

When the building is damaged, the natural frequencies can be obtained by using Matlab function "eig" with different values of stiffness. Fig.3.2.1.1 and Fig.3.2.1.2 show the variation .
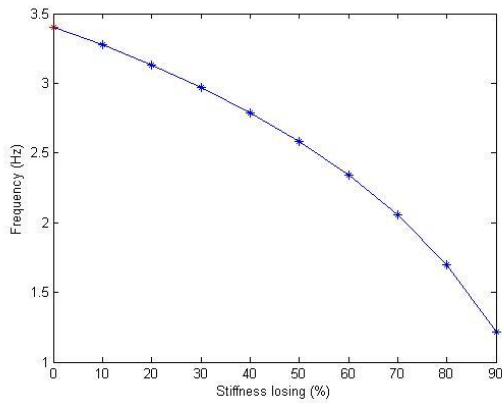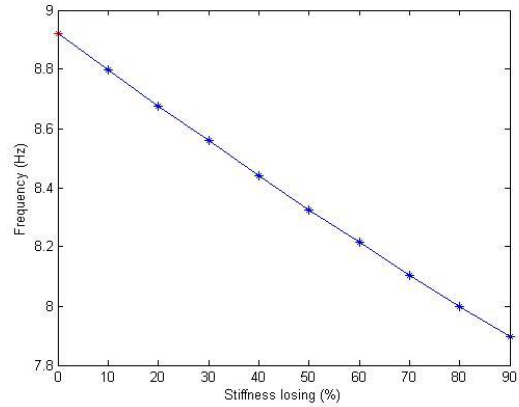
(a)   (b)

Fig.3.2.1.1 Frequency is decreasing with the stiffness loss of k_1.
(a) is for mode 1 and (b) is for mode 2
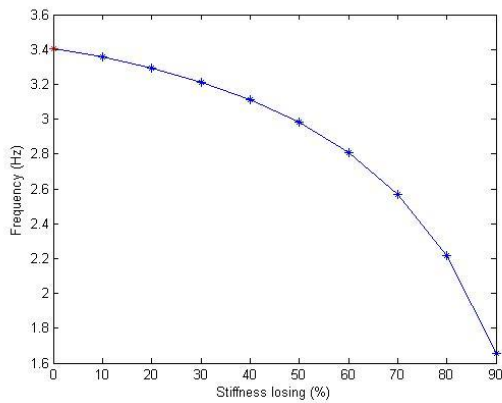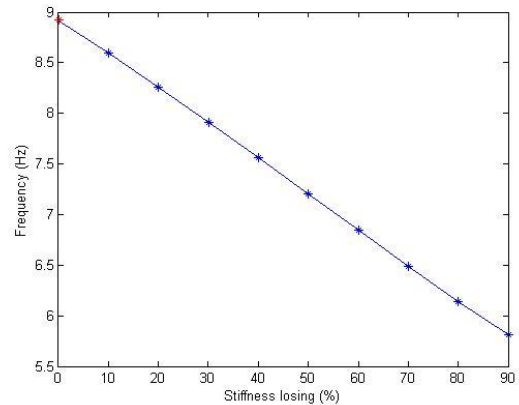
(a)   (b)

Fig.3.2.1.2 Frequency is decreasing with the stiffness loss of k_2.
(a) is for mode 1 and (b) is for mode 2

Since the natural frequencies are 3.4074 Hz and 8.9207 Hz when the building is under the

normal condition, the state vector which will generate the first kind of antigens G_1 is

(3.4074, 8.9207) or (0.3568, 0.9342) after normalization. The second kind of antigens G_2

is a set of the state vectors normalized from the values in Fig.3.2.1.1 and Fig.3.2.1.2.

After the trainings, the matured antibodies in the feature space of the natural frequencies

are shown in Figures 3.2.1.3 and 3.2.1.4, one for k_1-loss only and the other for k_2-loss

only.

Fig.3.2.1.3 Matured antibodies in the feature space of natural frequencies using the data from eigen-solution (k_1-loss only).
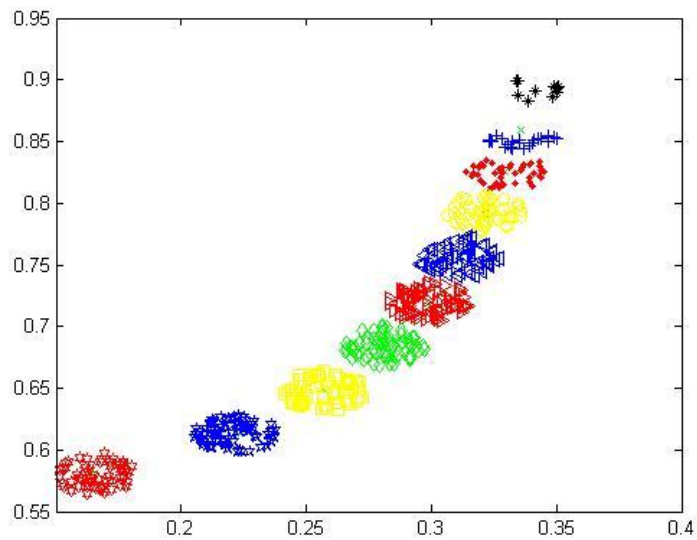
Fig.3.2.1.4 Matured antibodies in the feature space of natural frequencies using the data from eigen-solution (k_2-loss only).

(0.2689, 0.8383)
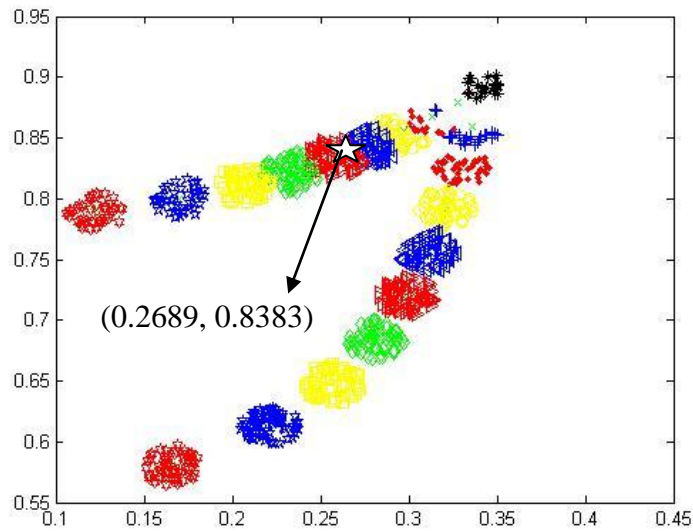
Fig.3.2.1.5 Comparison of the matured antibodies in the feature space of natural frequencies using the data from eigen-solution for k_1-loss and k_2-loss.

In Fig.3.2.1.5, the upper line is for k_1-loss only and the lower line is for k_2-loss only. The testing case of 45% k_1-loss is shown in the figure by a white star that is located roughly between the two groups of antibodies corresponding the 40% k_1-loss and 50% k_1-loss,

respectively. It is also observed that two lines representing the stiffness loss at different locations are well separated if the stiffness loss is more than 50% and merge when the stiffness loss is less than 20%, just similar to the database obtained by free-vibration data in Section 3.1.1. Thus the result from free-vibration data is usable when the natural frequency is used as feature space.

3.2.2 Using a modal shape as the feature space

Both abnormal and normal conditions of modal matrix Φ are obtained by solving

eigenvalue problem. Since $\Phi=[\underline{X}^{(1)}\ \underline{X}^{(2)}]=\begin{bmatrix} x_1^{(1)} & x_1^{(2)} \\ x_2^{(1)} & x_2^{(2)} \end{bmatrix}$, the ratio $x_1^{(1)}/x_2^{(1)}$ for modal

shape 1 should be fixed for each condition when different methods are using to calculate

it, and so do the ratio $x_1^{(2)}/x_2^{(2)}$ for modal shape 2. When the stiffness k_1 is losing, both of

the ratios are increasing, and the ratio $x_1^{(1)}/x_2^{(1)}$ for modal shape 1 is close to 1 while the

ratio $x_1^{(2)}/x_2^{(2)}$ for modal shape 2 is close to -1. That means, when k_1 is close to zero, the

structure of the vibration system is changed like a double-pendulum with a spring

between the two pendulums, which has the ratios 1 and -1. But when the stiffness k_2 is

losing, both of the ratios are decreasing, and the ratio $x_1^{(1)}/x_2^{(1)}$ for modal shape 1 is close

to zero while the ratio $x_1^{(2)}/x_2^{(2)}$ for modal shape 2 is close to minus infinity. Thus when

k_2 is close to zero, the structure of the vibration system is changed like a SDOF system,

which does not have any ratio. The variation of the ratios due to the stiffness loss is

shown in Fig.3.2.2.1 and Fig.3.2.2.2.
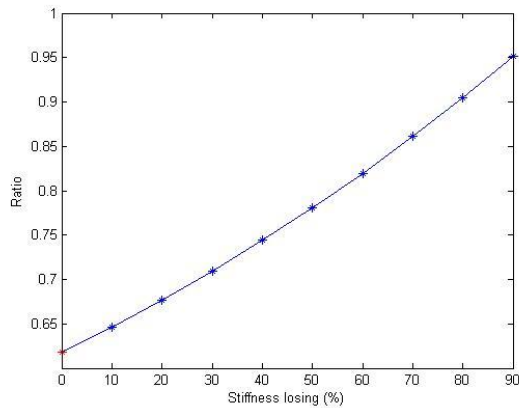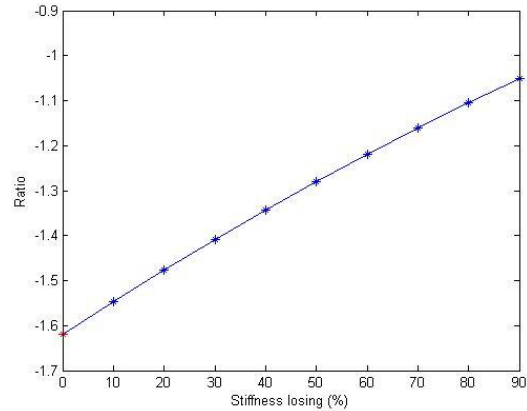
<center>(a)</center> <center>(b)</center>

Fig.3.2.2.1 Variation of the modal shape ratios due to the stiffness k_1-loss only with the data from eigen-solution.

(a) is $x_1^{(1)}/x_2^{(1)}$ for modal shape 1 and (b) is $x_1^{(2)}/x_2^{(2)}$ for modal shape 2
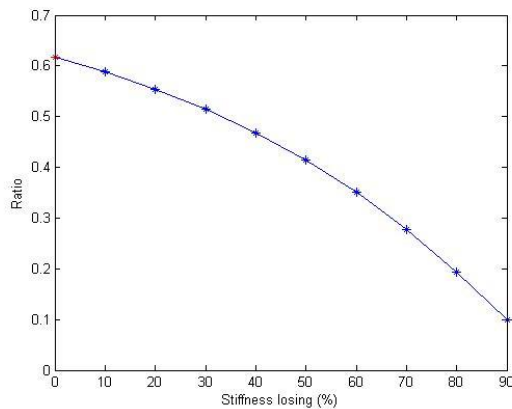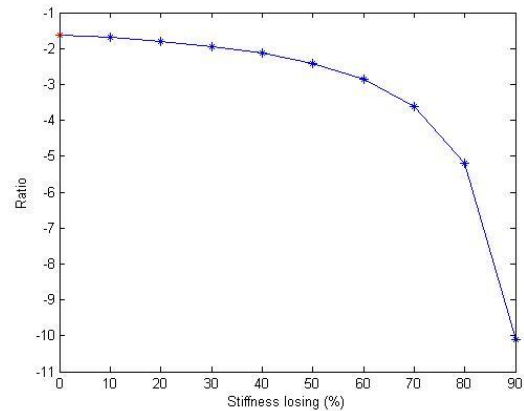
<center>(a)</center> <center>(b)</center>

Fig.3.2.2.2 Variation of the modal shape ratios due to the stiffness k_2-loss only with the data from eigen-solution.

(a) is $x_1^{(1)}/x_2^{(1)}$ for modal shape 1 and (b) is $x_1^{(2)}/x_2^{(2)}$ for modal shape 2

In the same way of Section 3.1.2, for modal shape 1, the state vector which will generate the first kind of antigens G_1 is (0.6180, 1) original or (0.5257, 0.8507) after normalization. The second kind of antigens G_2 generated as a large size of group of the normalized state vectors in the feature space, as shown in Fig.3.2.2.1 and Fig.3.2.2.2. After the trainings,

the matured antibodies are shown in figures 3.2.2.3 through 3.2.2.5.
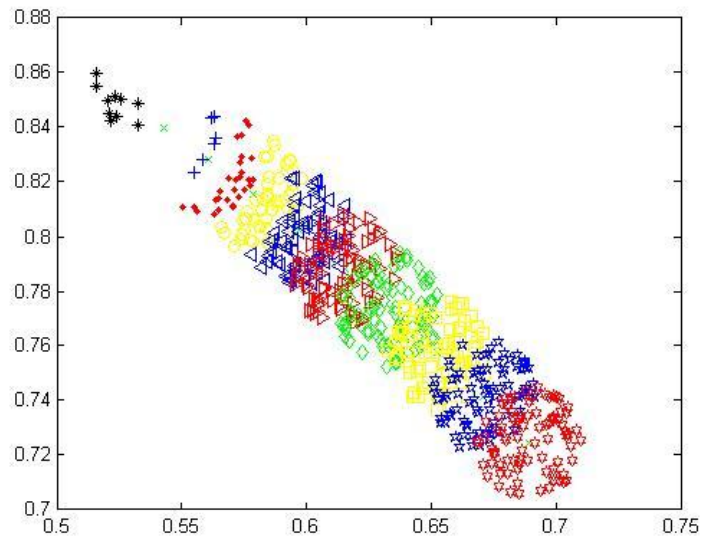
Fig.3.2.2.3 Matured antibodies in the feature space of modal shape 1 using the data from eigen-solution (k_1-loss only).
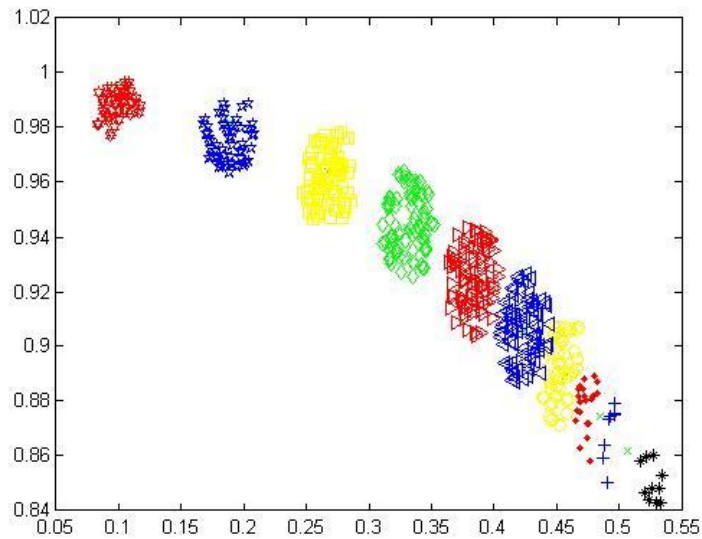
Fig.3.2.2.4 Matured antibodies in the feature space of modal shape 1 using the data from eigen-solution (k_2-loss only).
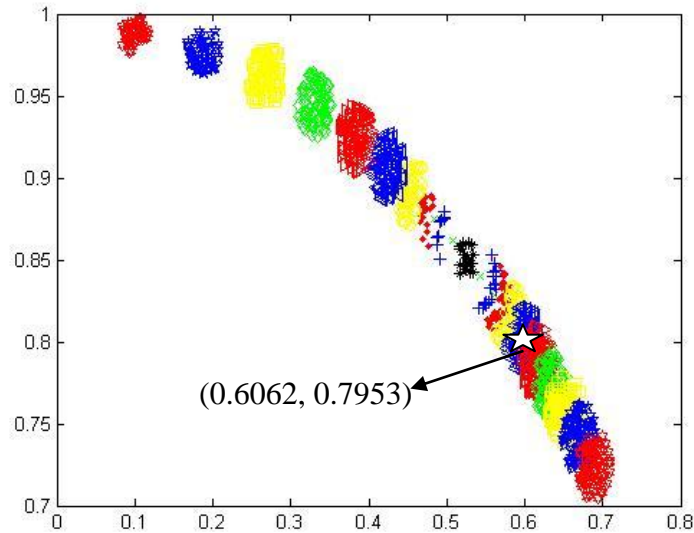
Fig.3.2.2.5 Comparison of the matured antibodies in the feature space of modal shape 1 using the data from eigen-solution for k_1-loss and k_2-loss.

In Fig.3.2.2.5, the lower line is for k_1, the upper line is for k_2, and the white star is the texting case of 45% k_1-loss. The lines of the antibodies for stiffness loss in different locations run the opposite directions, and this result is just like that from the free-vibration data. Thus, the result of modal shape 1 from the free-vibration data is usable.

For mode 2, the state vector which will generate the first kind of antigens G_1 is (-1.6190, 1) original, or (-0.8508, 0.5255) after normalization. The second kind of antigens G_2 is the state vectors normalized from the values in Fig.3.2.2.1 and Fig.3.2.2.2. After the trainings, the matured antibodies are shown in figures 3.2.2.6 through 3.2.2.8.

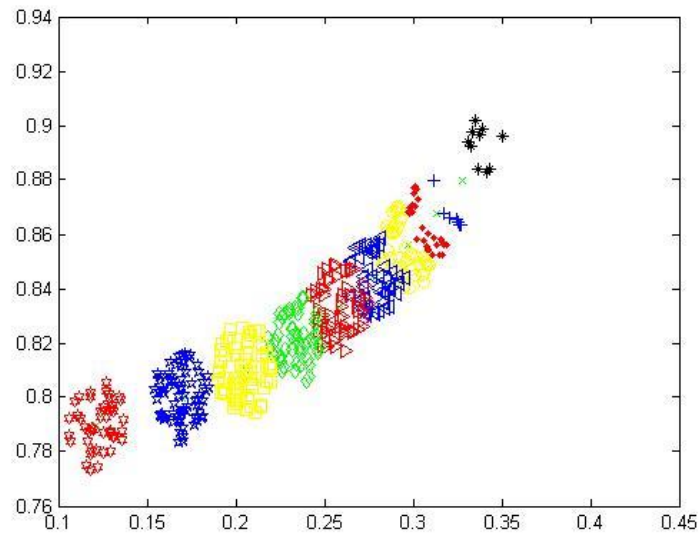Fig.3.2.2.6 Matured antibodies in the feature space of modal shape 2 using the data from eigen-solution (k_1-loss only).

Fig.3.2.2.7 Matured antibodies in the feature space of modal shape 2 using the data from eigen-solution (k_2-loss only).

Fig.3.2.2.8 Comparison of the matured antibodies in the feature space of modal shape 2 using the data from eigen-solution for k_1-loss and k_2-loss.

In Fig.3.2.2.8, the upper line is for k_1, the lower line is for k_2, and the white star is the texting case of 45% k_1-loss. It is observed that the matured antibodies are well separated as two lines those run the opposite directions. This result is better than that from free-vibration data in Section 3.1.1. But if all the results of frequency, modal shape 1 and modal shape 2 are considered, the results from free-vibration data are usable.

3.3 Study 3: Forced vibration data under seismic excitation

3.3.1 Using the natural frequencies as the feature space

When the building is under the normal condition, the natural frequencies are 3.41 Hz and 8.91 Hz which are shown in Fig.3.3.1.1 by using forced vibration data under seismic excitation.
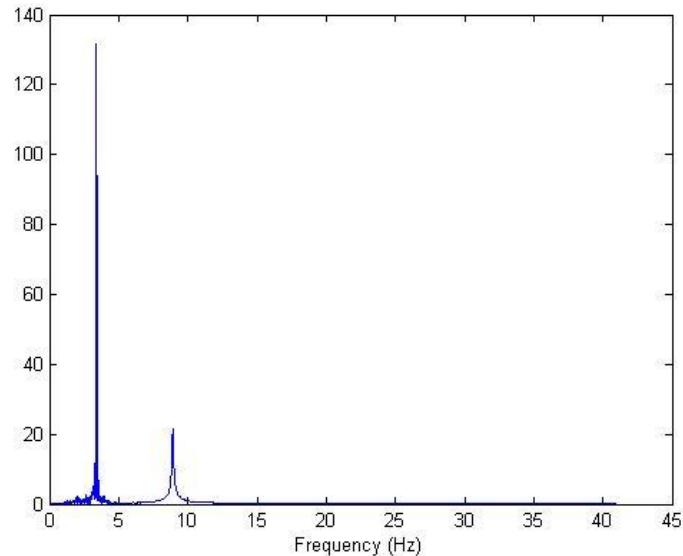
Fig.3.3.1.1 The Fourier response spectrum of a simulated forced vibration response of the healthy structure.

When the building is damaged, the values of the natural frequencies can be obtained and the variation is shown in Fig.3.3.1.2 and Fig.3.3.1.3. Since the seismic excitation might disturb the frequency, it is necessary to calculate the errors about the frequency for each condition. Compared with the natural frequencies of eigen-solution those mentioned in Section 3.2.1, the error for each frequency is in (-0.55%, 0.73%), see appendix A. Thus the frequencies from simulation are accurate enough.
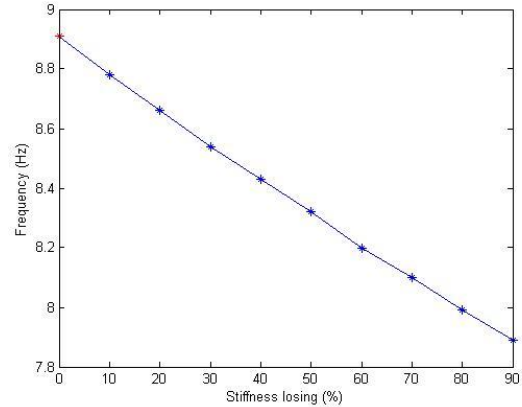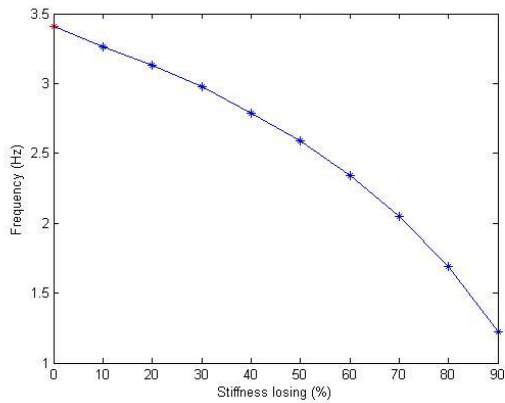
(a)   (b)

Fig.3.3.1.2 Frequency is decreasing with the stiffness loss of k_1.
(a) is for mode 1 and (b) is for mode 2
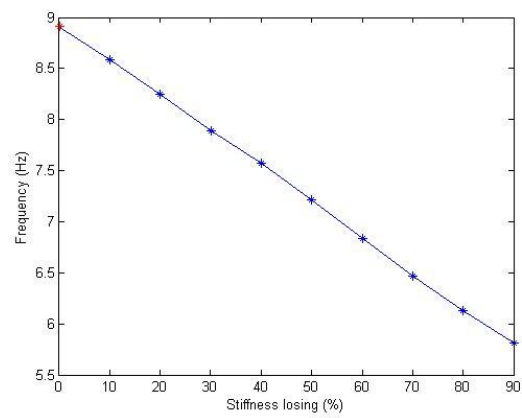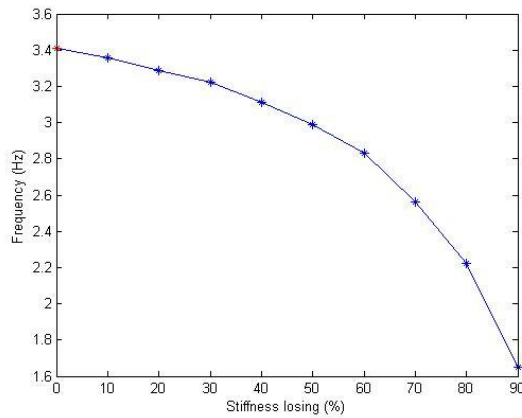
(a)   (b)

Fig.3.3.1.3 Frequency is decreasing with the stiffness loss of k_2.
(a) is for mode 1 and (b) is for mode 2

Since the natural frequencies are 3.41 Hz and 8.91 Hz when the building is under the normal condition, the state vector which will generate the first kind of antigens G_1 is (3.41, 8.91) original, or (0.341, 0.891) after normalization. The second kind of antigens G_2 is a set of the state vectors normalized from the values in Fig.3.3.1.2 and Fig.3.3.1.3. After the trainings, the matured antibodies are shown in the figures 3.3.1.4 through

3.3.1.6.
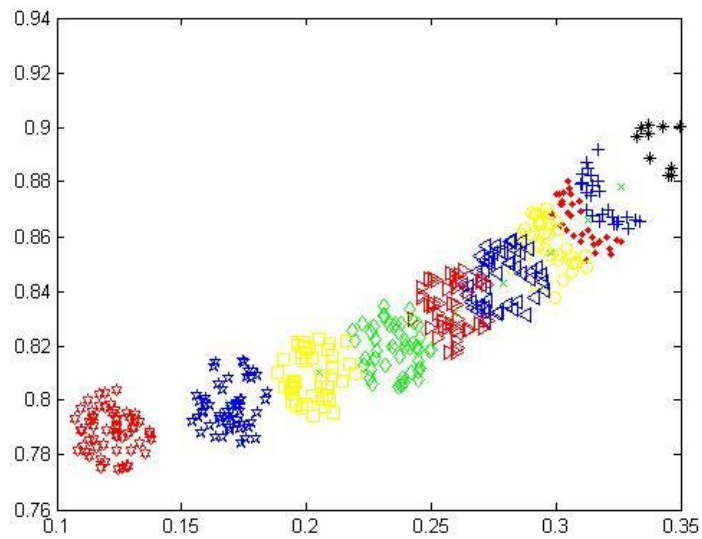
Fig.3.3.1.4 Matured antibodies in the feature space of natural frequencies using the forced vibration data (k_1-loss only).

Fig.3.3.1.5 Matured antibodies in the feature space of natural frequencies using the forced vibration data (k_2-loss only).
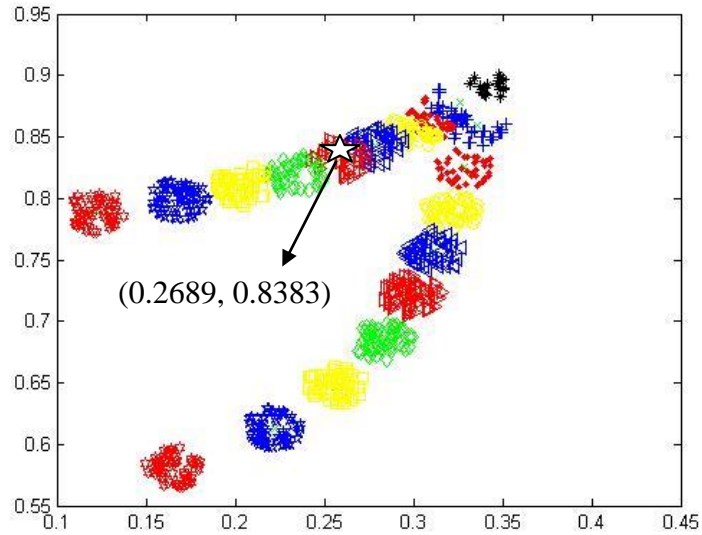
Fig.3.3.1.6 Comparison of the matured antibodies in the feature space of natural frequencies using the forced vibration data for k_1-loss and k_2-loss.

In Fig.3.3.1.6, the upper line is for k_1, the lower line is for k_2, and the white star is the texting case of 45% k_1-loss. It is observed that two lines representing the stiffness loss at different locations are well separated if the stiffness loss is more than 50% and merge if the stiffness loss is less than 20%, like the result in Sections 3.1.1 and 3.2.1. Thus the result of natural frequency from simulation data when the system is in earthquake is usable.

3.3.2 Using a modal shape as the feature space

Since the information of forced vibration data under seismic excitation is used, the parameters in the Matlab program should be chosen carefully. Similar with the Section 3.1.2, the first peak is at 3.41 Hz , i.e. the first natural frequency is at about the 341th point in Fig.3.3.1.1. Consider with the plot shape, the Gauss window is placed in the vicinity of the first peak from the 241th point to the 441th point on the plot, corresponding to N is 200 points in the Matlab function "gausswin(N, α)". To determine the value of α, this study tests the numbers from 1 to 50. For modal shape 1, the theoretical value of the ratio $x_1^{(1)}/x_2^{(1)}$ is 0.6180 when the building is under the normal condition. For each α, there are 8192 points along the length of the plot of time domain after the IFFT applying on the frequency domain. There are s_1 points which ratio is out of the range $(100\pm10)\%$ of 0.6180, the percentage of them is $ss_1=(s_1/8192)*100\%$. Usually, the result is usable if the percentage is less than 5%, and the smaller the percentage the better. A_1 is the average ratio for each α. The s_1, ss_1, and A_1 are corresponding to the data from displacements, while the corresponding parameters for velocities are s_2, ss_2, and A_2, and those for accelerations are s_3, ss_3, and A_3. These parameters are listed in the <u>appendix B</u>.

Most of "ss_1" and "ss_2" are less than 1%; all the "A_1" and "A_2" are near 0.61. But "ss_3" is up to 99%, most of "A_3" are in (0.7, 0.9). Thus the results form displacements and velocities are accurate enough, but the result from accelerations is unusable. When the "α"

is between [25, 35], the results are more accurate because $ss_1 < 0.2\%$, $ss_2 < 0.2\%$, A_1 and A_2

$\approx$ 0.618. If using moving average filter, the results are similar for the error of each point

is less than 1%. Using gausswin(200,30), and making the points j of the moving average

filter between [1, 50], the "A_1" and "A_2" are near 0.618, but the "ss_1" and "ss_2" is a little

more than these without moving average (the difference is only about 0.2%, see appendix

C). Thus moving average filter isn't necessary for modal shape 1.

In conclusion, when the building is under the normal condition, the ratio $x_1^{(1)}/x_2^{(1)}$ for

modal shape 1 is about 0.618. In this study, 0.6178 is chosen by using function

"gausswin(200,30)" without moving average filter. In the same way, when the building is

damaged, the ratios can be obtained, and Fig.3.3.2.1 shows the variation .

(a)   (b)
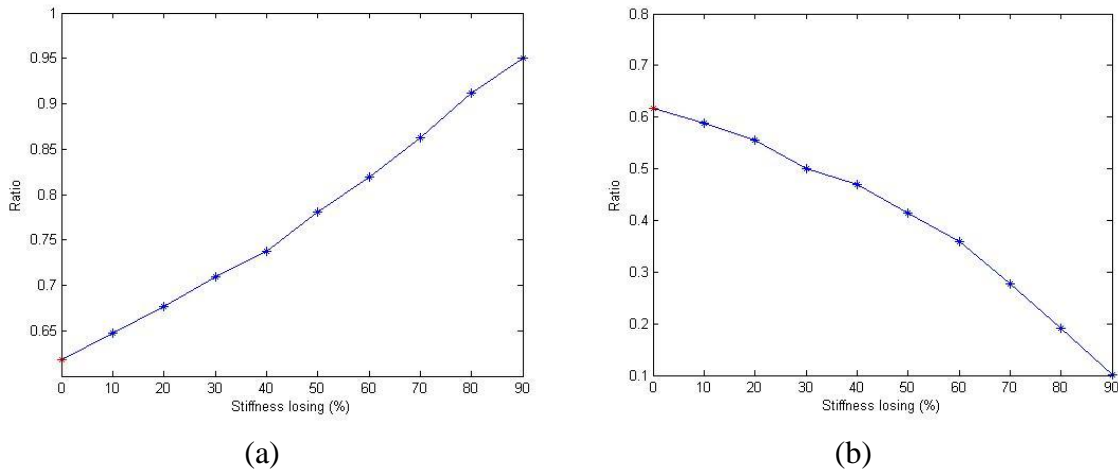
Fig.3.3.2.1 Variation of the modal shape ratio for mode 1 due to the stiffness from the
forced vibration data.
(a) is for k_1-loss and (b) is for k_2-loss

For modal shape 1, the state vector which will generate the first kind of antigens G_1 is

(0.6178, 1) original, or (0.5256, 0.8507) after normalization. The second kind of antigens

G_2 is the state vectors normalized from the values in Fig.3.3.2.1. After the trainings, the

matured antibodies are shown in the figures 3.3.2.2 through 3.3.2.4.
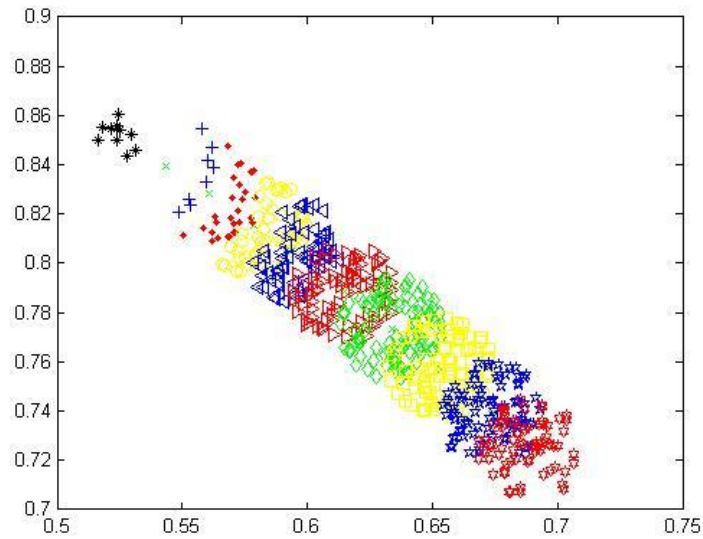
Fig.3.3.2.2 Matured antibodies in the feature space of modal shape 1 using the forced vibration data (k_1-loss only).
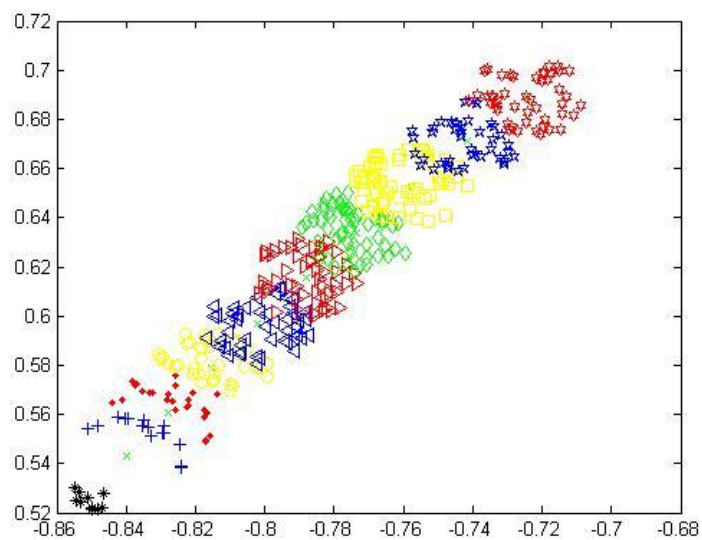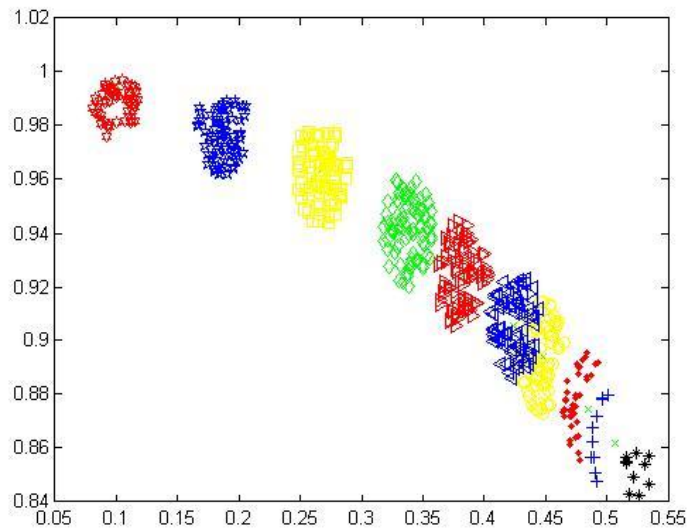
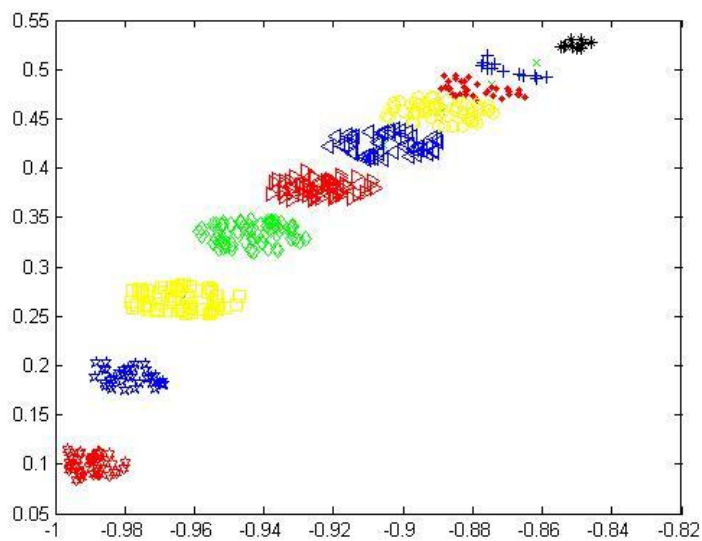

Fig.3.3.2.3 Matured antibodies in the feature space of modal shape 1 using the forced vibration data (k_2-loss only).
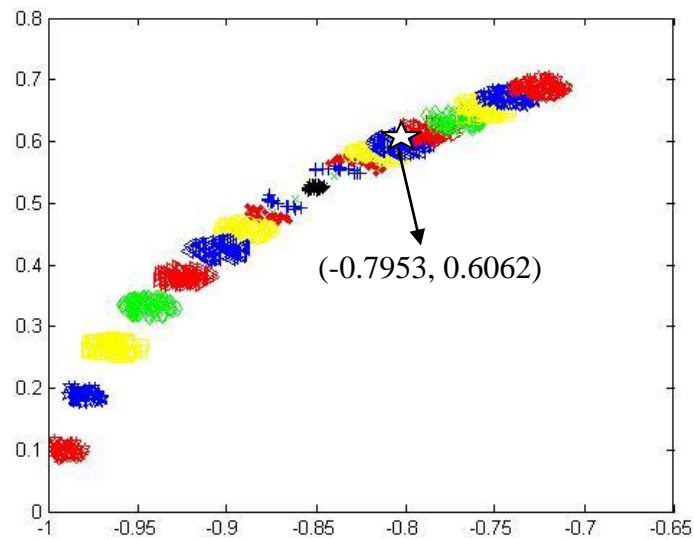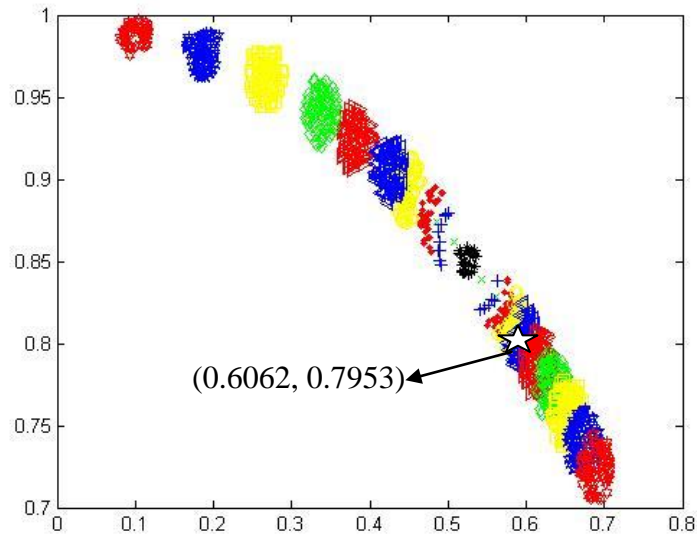
Fig.3.3.2.4 Comparison of the matured antibodies in the feature space of modal shape 1 using the forced vibration data for k_1-loss and k_2-loss.

In Fig.3.3.2.4, the lower line is for k_1, the upper line is for k_2, and the white star is the texting case of 45% k_1-loss. The two lines of the antibodies for stiffness loss in different locations run the opposite directions, which is just like that from the eigenvalue method. Thus, the result of modal shape 1 from the simulation data is usable.

For mode 2, the theoretical value of the ratio $x_1^{(2)}/x_2^{(2)}$ is -1.6190 when the building is under the normal condition. Like the mode 1, the parameters corresponding to the data from displacements are s_{12}, ss_{12}, and A_{12}; the corresponding parameters for velocities are s_{22}, ss_{22}, and A_{22}. (See appendix D). Since the result from accelerations is unusable for mode 1, the corresponding parameters for accelerations are not calculated. Using "gausswin(200, α)" (whereα=1, 2, …, 50), like mode 1, the percentage ss_{12}, ss_{22}, and the

average ratio A_{12}, A_{22} for mode 2 will be obtained, and listed in <u>appendix D</u> that shows

both ss_{12} and ss_{22} are bigger than 38%. Since the percentage should less than 5% and the

smaller the better, the result is unusable.

Since the initial conditions are $\underline{x}(0) = \underline{x}_0 = \underline{0}$ and $\underline{\dot{x}}(0) = \underline{v}_0 = \underline{0}$, the mode 1 is

dominated. Set $\underline{x}_0 = (0.1619, 0.1)'$, thus the mode 2 is dominated. Then using

"gausswin(200, α)" (where α=1, 2, …, 50) to calculate these parameters. The percentages

ss_{12} and ss_{22} are bigger than 16%, and this result is still unusable. Then using moving

average filter, the ss_{12} and ss_{22} are changed. Some of the percentages are decreasing, but

the lowest percentage 16% is increased to 25%. In this case, all the results of mode 2 are

unusable if the earthquake data are applied. In this case, this study tested the condition

when the system is in free vibration. The result in <u>appendix E</u> shows that all the

percentages are less than 0.2%, with the average ratios are around -1.61, and implies that

the biggest disturbance might from the earthquake data. To check this inference, this

study tested the condition when using "gausswin(200, 30)" and moving average filter

(from 1 to 50 points) with earthquake data. The percentages are bigger than 15% (see

<u>appendix F</u>) and prove that the earthquake data are the biggest disturbance. Thus, using

the condition when the system in free vibration to calculate the ratios $x_1^{(2)}/x_2^{(2)}$ for

modal shape 2 and the variation tendency of the ratios are shown in Fig.3.3.2.5.
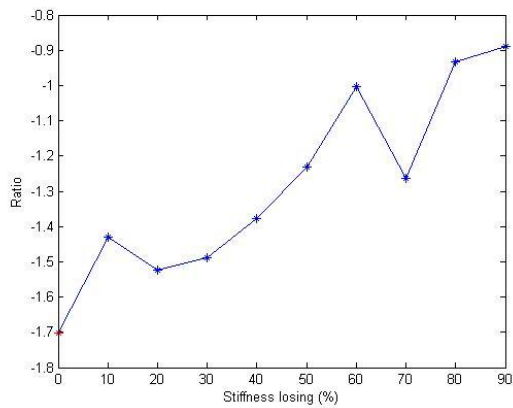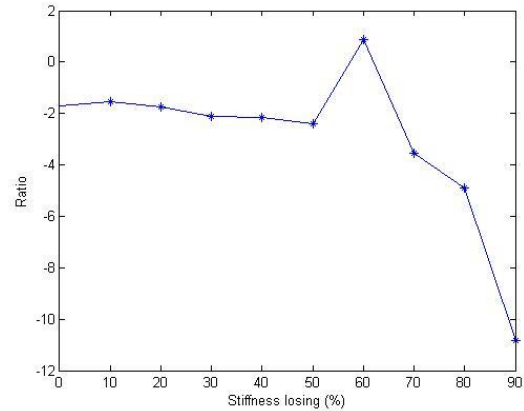
(a)   (b)

Fig.3.3.2.5 Variation of the modal shape ratio for mode 2 due to the stiffness from the forced vibration data.

(a) is for k_1-loss and (b) is for k_2-loss

In Fig.3.3.2.5, the lines are not smooth. Thus the antigens cannot train the antibodies accurately, and the result will not be as good as that from engienvalue method or even that of free-vibration. For mode 2, the state vector which will generate the first kind of antigens G_1 is (-1.7023, 1) original, or (-0.8622, 0.5065) after normalization. The second kind of antigens G_2 is a set of the state vectors normalized from the values in Fig.3.3.2.5. After the trainings, the matured antibodies are shown in the figures 3.3.2.6 through 3.3.2.8.
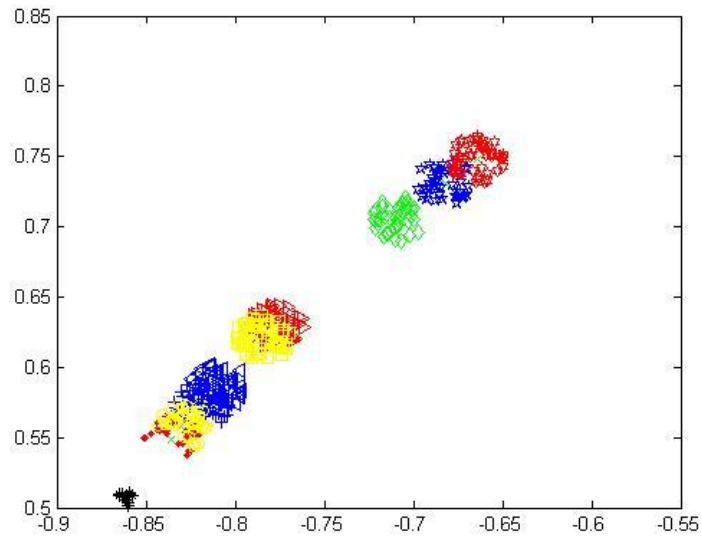
Fig.3.3.2.6 Matured antibodies in the feature space of modal shape 2 using the forced vibration data (k_1-loss only).
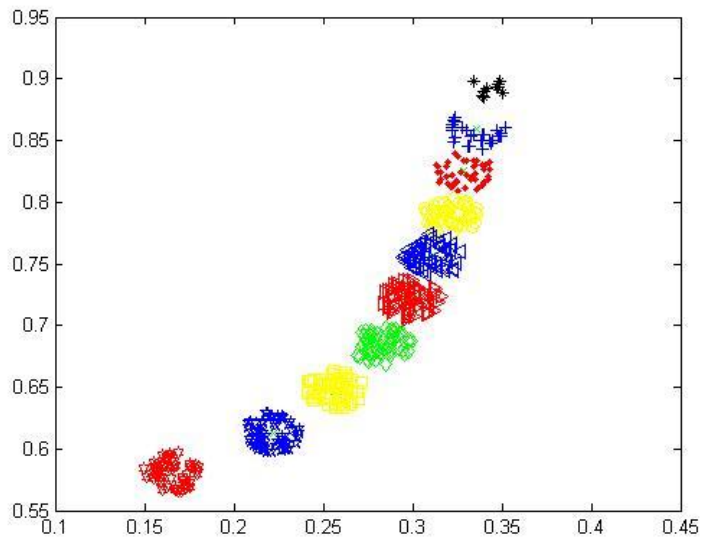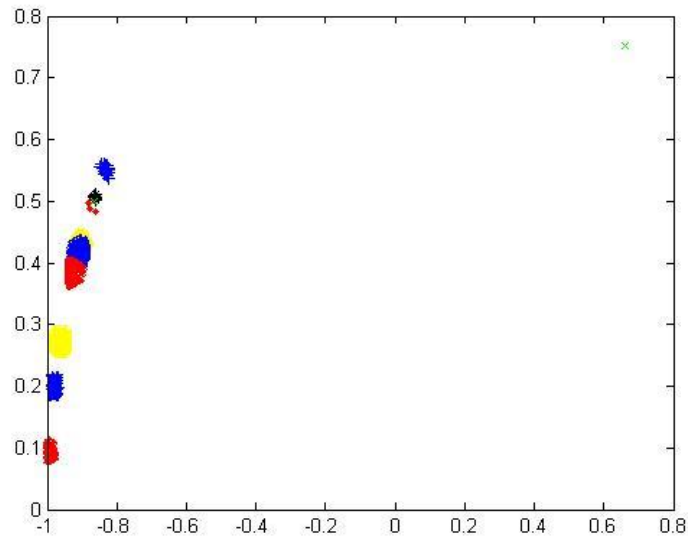

Fig.3.3.2.7 Matured antibodies in the feature space of modal shape 2 using the forced vibration data (k_2-loss only).

In Fig.3.3.2.7, one of the antigens is out of range. Thus it cannot train the antibodies. Another one of the antigens is also cannot train the antibodies, because it is in the area of normal condition.
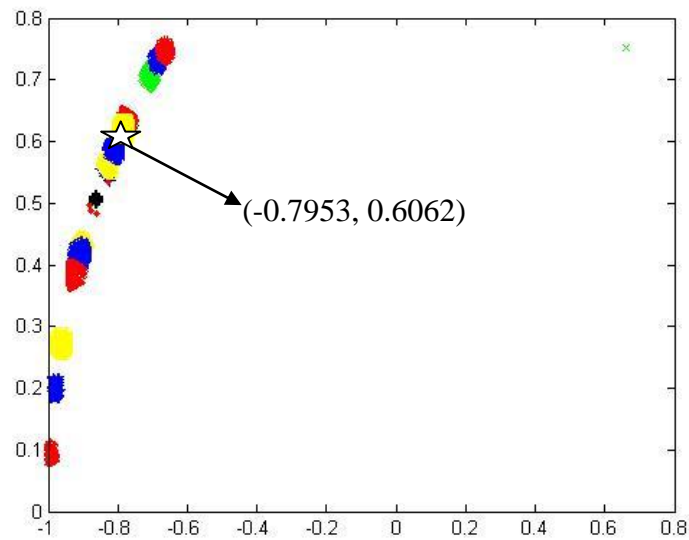
Fig.3.3.2.8 Comparison of the matured antibodies in the feature space of modal shape 2 using the forced vibration data for k_1-loss and k_2-loss.

In Fig.3.3.2.8, the upper line is for k_1, the lower line is for k_2, and the white star is the texting case of 45% k_1-loss. The general views of the above figures are like the figures from the eigenvalue method and the figures from free vibration. But some of the antigens are not usable, and not all the conditions are separate from each other, thus this result is unusable.

In the actual situation, the earthquake excitation will disturb the result for mode 2, and mode 2 is not dominated. Thus the simulation method in this paper is not accurate enough. In this case, a new method or feature space needs to be found.

4 Conclusions

As illustrated for the linear 2DOF mass-spring-damper system, the Artificial Immune System (AIS)-based Structural Health Monitoring (SHM) algorithm developed in this thesis can be successfully applied to detect structural damage due to stiffness loss and if damage occurred, also to identify the location and to assess the extent of the damage. Both the natural frequency and the modal shapes of the system were respectively selected as the feature space for this methodology. Simulated free-vibration data and seismic response data were used in the training process. Consistently good results were obtained in all the cases investigated except only a couple of cases where the modal shape 2 was selected as the feature space and the database was trained by the seismic response data. In these cases, significant errors may be attributed to the incapability of extracting the modal shape 2 due to the irregularity of the seismic input and insignificance of the 2nd modal response. As compared to some early results in the literature, the antibody detectors due to damage at different locations were well separated, which makes the damage allocation much easier.

Future work can be suggested to extend the application and to improve the performance of this AIS-based SHM technique. Other feature spaces that are sensitive to the structural loss may be explored. In the case of a large-scale linear MDOF system where the number of DOF is much greater than 2, selection of the feature space remains a challenge.

Including only a limited number of modes would make the result inaccurate but on the other hand increasing the dimension of the feature space will lead to unaffordable computational efforts. The effects of measurement noise and modeling effort may also need investigated.

5 References

[1] Hoon Sohn, Charles R. Farrar, Francois Hemez, Jerry Czarnecki. *A Review of Structural Health Monitoring Literature* 1996-2001.

[2] Dawson, Brian (1976). Vibration condition monitoring techniques for rotating machinery. *The Shock and Vibration Digest* (London: SpingerLink) 8 (12): 3.

[3] E. A. Johnson, H. F. Lam; L. S. Katafygiotis, J. L. Beck. Phase I IASC-ASCE Structural Health Monitoring Benchmark Problem Using Simulated Data, *Journal of Engineering Mechanics © ASCE / January* 2004, 3-15.

[4] C.K. Lau, W.P.N. Mak, K.Y. Wong, W.Y.K. Chan, K.L.D. Man Structural health monitoring of three cable-supported bridges in Hong Kong F.K. Chang (Ed.), *Structural health monitoring*, Technomic, Lancaster (PA) (1999), 450–460.

[5] K.Y. Wong, Instrumentation and health monitoring of cable-supported bridges, *Structural Control and Health Monitoring*, 11 (2) (2004), 91–124.

[6] Andersen EY, Pedersen L. Structural monitoring of the Great Belt East Bridge. Krokebogr J, editor. Strait crossings 94. Rotterdam: Balkema; 1994. 189–95.

[7] Myrvoll F, Aarnes KA, Larssen RM, Gjerding-Smith K. Full scale measurements for design verification of bridges. Proceedings of the 18th international modal analytical conference. Bethel (CT): Society for Experimental Mechanics; 2000. 827–35.

[8] Brownjohn JMW. Lessons from monitoring the performance of highway bridges. In: Proceedings of the international workshop on advanced sensors, structural health monitoring and smart structures. 2003 [CD-ROM].

[9] Casciati F. An overview of structural health monitoring expertise within the European Union. In: Wu ZS, Abe M, editors. *Structural health monitoring and intelligent infrastructure*. Lisse: Balkema; 2003. p. 31–7.

[10] Pines DJ, Aktan AE. Status of structural health monitoring of longspan bridges in the United States. Progress in Structural Engineering and Materials 2002; 4(4):372–80.

[11] Wang ML. State-of-the-art applications in health monitoring. Invited presentation to workshop on basics of structural health monitoring and optical sensing technologies in civil engineering. Taiwan: National Central University; 2004. 113–42.

[12] Cheung MS, Naumoski N. The first smart long-span bridge in Canada—health

monitoring of the Confederation Bridge. In: Mufti AA, editor. *Proceedings of the 1st international workshop on structural health monitoring of innovative civil engineering structures*. Winnipeg: ISIS Canada Corporation; 2002. 31–44.

[13] Mufti AA. Structural health monitoring of innovative Canadian civil engineering structures. *Structural Health Monitoring* 2002; 1(1): 89–103.

[14] Wu ZS. Structural health monitoring and intelligent infrastructures in Japan. Wu ZS, Abe M, editors. *Structural health monitoring and intelligent infrastructure*. Lisse: Balkema; 2003. 153–67.

[15] Fujino Y, Abe M. Structural health monitoring—current status and future. Boller C, Staszewski WJ, editors. Proceedings of the 2nd European workshop on structural health monitoring. Lancaster (PA): DEStech; 2004. 3–10.

[16] Koh HM, Choo JF, Kim SK, Kim CY. Recent application and development of structural health monitoring systems and intelligent structures in Korea. Wu ZS, Abe M, editors. *Structural health monitoring and intelligent infrastructure*. Lisse: Balkema; 2003. 99–111.

[17] Yun CB, Lee JJ, Kim SK, Kim JW. Recent R&D activities on structural health monitoring for civil infra-structures in Korea. *KSCE Journal of Civil Engineering* 2003; 7(6):637–51.

[18] Xiang HF. Health monitoring status of long-span bridges in China, Proceedings of the workshop on research and monitoring of long span bridge. 2000, 24–31.

[19] Ou J. The state-of-the-art and application of intelligent health monitoring systems for civil infrastructures in mainland of China. Zingoni A, editor. *Progress in structural engineering, mechanics and computation*. London: AA Balkema/Taylor and Francis; 2004. 599–608 [CD-ROM].

[20] Nigbor RL, Diehl JG. Two years' experience using OASIS realtime remote condition monitoring system on two large bridges. Chang FK, editor. *Structural health monitoring: current status and perspectives*. Lancaster (PA): Technomic; 1997. 410–7.

[21] Thomson P, Marulanda Casas J, Marulanda Arbelaez J, Caicedo J. Real time health monitoring of civil infrastructure systems in Colombia. Chase SB, Aktan AE, editors. Health monitoring and management of civil infrastructure systems. Bellingham (WA): The International Society for Optical Engineering; 2001. 113–21.

[22] National Highways Authority of India (NHAI). Instrumentation (structural monitoring system) for Yamuna Bridge at Allahabad/Naini. Tender document; 2002.

Available at http://www.nhai.org/NIT.htm .

[23] JP Ou , Some recent advances of intelligent health monitoring systems for civil infrastructures in mainland China, *Structural health monitoring and intelligent infrastructure*, 130

[24] M. C¸elebi, M.EERI, A. Sanli, M. Sinclair, S. Gallant, and D. Radulescu. Real-Time Seismic Monitoring Needs of a Building Owner—and the Solution: A Cooperative Effort.

[25] C. B. Van Way, J. N. Kudva, J. N. Schoess, M. L Zeigler, J. M. Alper. Aircraft structural health monitoring system development-overview of the Air Force/Navy Smart Metallic Structures program.

[26] Jamie Twycross and Uwe Aickelin. Biological Inspiration for Artificial Immune Systems.

[27] Donald E. Goodman JR, Lois C. Boggess, Andrew B. Watkins. Artificial immune system classification of multiple-class problems.

[28] Charles Janeway (2001). *Immunobiology*. (5th ed.). Garland Publishing. ISBN 0-8153-3642-X.

[29] Litman GW, Rast JP, Shamblott MJ, Haire RN, Hulst M, Roess W, Litman RT, Hinds-Frey KR, Zilch A, Amemiya CT (January 1993). Phylogenetic diversification of immunoglobulin genes and the antibody repertoire. Mol. Biol. Evol. 10 (1): 60–72.

[30] http://en.wikipedia.org/wiki/Antibody .

[31] U. Aickelin and D. Dasgupta. Artificial Immune Systems. *Search Methodologies: Introductory Tutorials in Optimization and Decision Support Techniques*. Chapter 13.

[32] http://en.wikipedia.org/wiki/Cloning.

[33] de Castro, Leandro N.; Timmis, Jonathan (2002). *Artificial Immune Systems: A New Computational Intelligence Approach*. Springer. pp. 57–58.

[34] Dasgupta, D. Artificial Immune System (AIS) as a branch of Computational Intelligence (CI).

[35] Chen Qiang, Zheng Deling, Li Xiangping. Faults Diagnosis Model Based on Artificial Immunity and its Application.

[36] Leandro Nunes de Castro, and Fernando José Von Zuben. Artificial Immune Systems:

Part II – a Survey of Applications.

[37] Leandro Nunes de Castro, Fernando J. Von Zuben. The Clonal Selection Algorithm with Engineering Applications.

[38] Forrest, S.; Perelson, A.S.; Allen, L.; Cherukuri, R. (1994). "Self-nonself discrimination in a computer" (PDF). *Proceedings of the 1994 IEEE Symposium on Research in Security and Privacy*. Los Alamitos, CA. 202–212. http://www.cs.unm.edu/~immsec/publications/virus.pdf.

[39] http://en.wikipedia.org/wiki/Artificial_immune_system#cite_note-1.

[42] Xueguang Shao, Zonghai Chen, Xiangqin Lin. Resolution of multicomponent overlapping chromatogram using an immune algorithm and genetic algorithm. *Chemometrics and Intelligent Laboratory Systems* 50 (2000). 91–99

[41] Satoshi Endoh, Naruaki Toma, koji Yamada. Immune algorithm for n-TSP.

[42] Jang-Sung Chun, Min-Kyu Kim, Hyun-Kyo Jung, Sun-Ki Hong. Shape Optimization of electromagnetic devices using Immune Algorithm.

[43] Dipankar Dasgupta, Stephanie Forrest. Artificial Immune Systems in Industrial Applications.

[44] Paul K. Harmer, Paul D. Williams, Gregg H. Gunsch, Gary B. Lamont. An Artificial Immune System Architecture for Computer Security Applications. *IEEE Transactions on Evolutionary Computation*, VOL. 6, NO. 3, June 2002, 252-280.

[45] D. Dasgupta. Immune-based intrusion detection system: a general framework. In Proceedings of the 22"" national inforniation svsrems security conferencfi (NISSC). I999.

[46] S. Hofmeyr and S. Forrest. Architecture for an artificial immune system, *Evolutionary Compuiation*, vol. 8, no. 4. 2000. 443-473.

[47] Tom Morrison, Uwe Aickelin. An Artificial Immune System as a Recommender for Web Sites.

[48] Jing Yu, Feng Wang. Simulation Modeling of Network Intrusion Detection Based on Artificial Immune System. *2010 Second WRI World Congress on Software Engineering*. 145-148.

[49] Kazuhiko Takahashi, Takayuki Yamada. Application of an Immune Feedback Mechanism to Control Systems.

[50] K. Krishnakumar and J. Neidhoefer. Immunized adaptive critic for an autonomous aircraft control application. *Artificial Immune Systems and Their Applications*. New York: Springer-Verlag, 1999, 221–241.

[51] Jie Wu, Jiong Shen, Yiguo Li. Design of the immune control system for thermal engineering process and its stability analysis.

[52] F.G.R. Guimaraes, M. Palhares, F. Campelo, H. Igarashi. Design of mixed control systems using algorithms inspired by the immune system. *Information Sciences*, 177 (2007), 4368–4386.

[53] Fangwei Xie, Youfu Hou, Zhipeng Xu, Rui Zhao. Fuzzy-immune control strategy of a hydro-viscous soft start device of a belt conveyor. *Mining Science and Technology*. 19 (2009). 0544–0548.

[54] P. J. Costa Branco, J. A. Dente, R. Vilela Mendes. Using Immunology Principles for Fault Detection. *IEEE Transactions on Industrial Electronics*, VOL.50, NO. 2, April 2003, 362-373.

[55] D. W. Bradley and A. M. Tyrrell, Immunotronics: Hardware fault tolerance inspired by the immune system.Proc. 3rd Int. Conf. Evolvable Syst. (ICES 2000), 2000, 11–20.

[56] C.A. Laurentys, G. Ronacher, R.M. Palhares, W.M. Caminhas. Design of an Artificial Immune System for fault detection: A Negative Selection Approach. *Expert Systems with Applications*. Volume 37, Issue 7, July 2010, 5507–5513.

[57] Z. Chilenguea, J.A. Denteb, P.J. Costa Branco. An artificial immune system approach for fault detection in the stator and rotor circuits of induction machines. *Electric Power Systems Research*. Volume 81, Issue 1, January 2011, 158–169.

[58] C.A. Laurentys, R.M. Palhares, W.M. Caminhas. Design of an artificial immune system based on Danger Model for fault detection. *Expert Systems with Applications*. Volume 37, Issue 7, July 2010, 5145–5152.

[59] Ilhan Aydin, Mehmet Karakose, Erhan Akin. Chaotic-based hybrid negative selection algorithm and its applications in fault and anomaly detection. *Expert Systems with Applications*. Volume 37, Issue 7, July 2010, 5285–5294.

[60] Bo Chen. Artificial-immune-system approach enables monitoring structural health.

[61] A.K. Pandey, M. Biswas, Damage Detection in Structures Using Changes in Flexibility, *Journal of Sound and Vibration*, Volume 169, Issue 1, 6 January 1994, 3–17.

[62] B.R. Ellis, A.J. Bougard. Dynamic testing and stiffness evaluation of a six-storey timber framed building during construction. *Engineering Structures* 23 (2001) 1232–1242.

[63] Zhuo Wang, Weiming Yan, Yunda Shao. Three-Step Method for Stiffness Identification of Inter-Story Shearing Structures Under Ambient Excitation. *Tsinghua Science and Technology*. Volume 14, Number S2, December 2009, 69-74.

[64] Ebrahim Khanmirza, Naser Khaji, Vahid Johari Majd. Ebrahim Khanmirza, Naser Khaji, Vahid Johari Majd. *Expert Systems with Applications* 38 (2011) 5320–5329.

[65] Amos Gilat, Vish Subramanian. *Numerical Methods for Engineerings and Sciences: An Introduction with Applications Using MATLAB*, Second Edition. 347-354.

[66] http://www.strongmotioncenter.org/cgi-bin/CESMD/iqr_dist_DM2.pl?IQRID=Calexico_14Sep2010&SFlag=0&Flag=2.

Appendix

Appendix A The errors of natural frequencies identified from the seismic response data

Damage location Errors (%) Stiffness losing (%)	First-story stiffness loss		Second-story stiffness loss	
	Mode 1	Mode 2	Mode 1	Mode 2
0	0.0763	-0.1199	0.0763	-0.1199
10%	-0.5370	-0.2057	0.1311	-0.0419
20%	-0.1021	-0.1971	-0.0699	-0.0945
30%	0.2793	-0.2103	0.1960	-0.2970
40%	0.0215	-0.1303	-0.1220	0.1124
50%	0.3332	-0.0757	0.2078	0.0902
60%	-0.0171	-0.1741	0.7297	-0.0365
70%	-0.1996	-0.0629	-0.2999	-0.2143
80%	-0.5531	-0.1125	0.2031	-0.0929
90%	0.2218	-0.0785	-0.2961	0.0275

Appendix B　Comparison of accuracy in extracting mode 1, using the Gauss Windows (gausswin(200, α)) with different α for the seismic response data

α	ss_1	A_1	α	ss_2	A_2	α	ss_3	A_3
1.0000	1.0986	0.6187	1.0000	1.0254	0.6172	1.0000	99.3896	0.9830
2.0000	0.9521	0.6199	2.0000	1.0620	0.6195	2.0000	97.2046	0.9071
3.0000	0.6836	0.6179	3.0000	0.6348	0.6185	3.0000	71.7041	1.3372
4.0000	0.5737	0.6172	4.0000	0.5493	0.6166	4.0000	48.8281	0.7587
5.0000	0.5737	0.6179	5.0000	0.4761	0.6172	5.0000	48.2544	0.8176
6.0000	0.4272	0.6175	6.0000	0.3296	0.6176	6.0000	48.6694	0.7988
7.0000	0.3906	0.6156	7.0000	0.3784	0.6179	7.0000	49.0967	0.8001
8.0000	0.3784	0.6087	8.0000	0.2563	0.6157	8.0000	49.8413	0.8147
9.0000	0.2808	0.6198	9.0000	0.2441	0.6179	9.0000	50.5981	0.7977
10.0000	0.2197	0.6179	10.0000	0.2808	0.6173	10.0000	51.3672	0.8061
11.0000	0.2563	0.6188	11.0000	0.2930	0.6178	11.0000	52.1362	0.7568
12.0000	0.2686	0.6169	12.0000	0.3296	0.6180	12.0000	52.9175	0.8255
13.0000	0.3784	0.6177	13.0000	0.5005	0.6190	13.0000	53.6987	0.7926
14.0000	0.3052	0.6193	14.0000	0.4272	0.6180	14.0000	54.4189	0.8033
15.0000	0.2319	0.6185	15.0000	0.3174	0.6175	15.0000	55.1758	0.7726
16.0000	0.2319	0.6183	16.0000	0.3052	0.6179	16.0000	56.1523	0.8564
17.0000	0.2686	0.6176	17.0000	0.2563	0.6156	17.0000	56.8848	0.8349
18.0000	0.2686	0.6176	18.0000	0.2563	0.6187	18.0000	57.5684	0.8768
19.0000	0.2930	0.6178	19.0000	0.3296	0.6177	19.0000	58.2397	1.1712
20.0000	0.3052	0.6180	20.0000	0.2197	0.6179	20.0000	59.0820	0.8845
21.0000	0.1831	0.6176	21.0000	0.2197	0.6180	21.0000	59.9365	0.6221
22.0000	0.1709	0.6183	22.0000	0.2319	0.6178	22.0000	60.6934	0.8382
23.0000	0.2075	0.6179	23.0000	0.1953	0.6181	23.0000	61.5479	0.8286
24.0000	0.1953	0.6180	24.0000	0.2075	0.6182	24.0000	62.1704	0.8194
25.0000	0.1221	0.6181	25.0000	0.1831	0.6181	25.0000	62.9272	0.8261
26.0000	0.1831	0.6184	26.0000	0.1587	0.6180	26.0000	63.5620	0.8717
27.0000	0.1465	0.6187	27.0000	0.1831	0.6174	27.0000	64.2334	0.6680
28.0000	0.1465	0.6183	28.0000	0.1465	0.6180	28.0000	64.8682	0.7374
29.0000	0.1709	0.6180	29.0000	0.1587	0.6180	29.0000	65.4785	0.8113
30.0000	0.1587	0.6171	30.0000	0.1465	0.6177	30.0000	66.0889	-1.9684
31.0000	0.1587	0.6179	31.0000	0.1709	0.6193	31.0000	66.7358	0.3858
32.0000	0.1343	0.6175	32.0000	0.1709	0.6179	32.0000	67.7490	0.8622

33.0000	0.1221	0.6179	33.0000	0.1221	0.6177	33.0000	68.3228	0.8758
34.0000	0.1099	0.6179	34.0000	0.1587	0.6181	34.0000	69.1528	0.8421
35.0000	0.1221	0.6180	35.0000	0.1587	0.6179	35.0000	70.0562	0.8250
36.0000	0.1587	0.6179	36.0000	0.1343	0.6180	36.0000	70.7764	0.8233
37.0000	0.2075	0.6175	37.0000	0.1221	0.6179	37.0000	71.3013	1.0182
38.0000	0.2563	0.6175	38.0000	0.1221	0.6179	38.0000	72.3999	0.7501
39.0000	0.2808	0.6238	39.0000	0.1465	0.6179	39.0000	73.2666	0.8229
40.0000	0.3174	0.6177	40.0000	0.1099	0.6182	40.0000	73.8770	0.8149
41.0000	0.3174	0.6178	41.0000	0.1343	0.6184	41.0000	74.5605	0.8895
42.0000	0.3174	0.6176	42.0000	0.2197	0.6181	42.0000	75.0977	0.8497
43.0000	0.3052	0.6176	43.0000	0.2808	0.6174	43.0000	75.9644	0.7906
44.0000	0.3418	0.6173	44.0000	0.2808	0.6174	44.0000	76.7090	0.8152
45.0000	0.3662	0.6172	45.0000	0.2808	0.6187	45.0000	77.4658	1.0586
46.0000	0.3784	0.6190	46.0000	0.3174	0.6179	46.0000	78.0884	0.8012
47.0000	0.3906	0.6184	47.0000	0.3174	0.6178	47.0000	78.6255	0.7913
48.0000	0.3906	0.6163	48.0000	0.3540	0.6174	48.0000	79.5044	0.7738
49.0000	0.4517	0.6171	49.0000	0.3418	0.6172	49.0000	80.2124	0.7814
50.0000	0.4517	0.6113	50.0000	0.3784	0.6174	50.0000	81.1157	0.6491

Appendix C Comparison of accuracy in extracting mode 1, using j point moving average filter with different j for the seismic response data (when using gausswin(200,30))

j	ss_1	A_1	j	ss_2	A_2
1.0000	0.1587	0.6171	1.0000	0.1465	0.6177
2.0000	0.2319	0.6173	2.0000	0.2686	0.6180
3.0000	0.1587	0.6180	3.0000	0.1831	0.6180
4.0000	0.4150	0.6184	4.0000	0.4883	0.6185
5.0000	0.4150	0.6197	5.0000	0.5005	0.6171
6.0000	0.6592	0.6199	6.0000	0.5615	0.6171
7.0000	0.3906	0.6172	7.0000	0.3174	0.6177
8.0000	0.2441	0.6177	8.0000	0.2319	0.6174
9.0000	0.3906	0.6177	9.0000	0.3540	0.6080
10.0000	0.6714	0.6142	10.0000	0.8179	0.6206
11.0000	0.3662	0.6166	11.0000	0.4028	0.6186
12.0000	0.3418	0.6183	12.0000	0.3906	0.6185
13.0000	0.4028	0.6340	13.0000	0.4517	0.6523
14.0000	0.5005	0.6206	14.0000	0.5127	0.6179
15.0000	0.6348	0.6140	15.0000	0.6592	0.6184
16.0000	0.6470	0.6193	16.0000	0.6104	0.6166
17.0000	0.4517	0.6171	17.0000	0.3906	0.6180
18.0000	0.2441	0.6186	18.0000	0.2075	0.6174
19.0000	0.1465	0.6184	19.0000	0.1343	0.6182
20.0000	0.1831	0.6182	20.0000	0.1831	0.6183
21.0000	0.2441	0.6190	21.0000	0.2930	0.6179
22.0000	0.4150	0.6188	22.0000	0.3662	0.6194
23.0000	0.4272	0.6183	23.0000	0.4639	0.6182
24.0000	0.5371	0.6233	24.0000	0.5371	0.6184
25.0000	0.4761	0.6180	25.0000	0.4517	0.6191
26.0000	0.1831	0.6179	26.0000	0.2197	0.6179
27.0000	0.1343	0.6175	27.0000	0.0610	0.6181
28.0000	0.0977	0.6184	28.0000	0.1221	0.6182
29.0000	0.1953	0.6241	29.0000	0.2197	0.6182
30.0000	0.3052	0.6182	30.0000	0.2808	0.6176
31.0000	0.4395	0.6186	31.0000	0.3784	0.6187
32.0000	0.4028	0.6179	32.0000	0.4395	0.6183

33.0000	0.5737	0.6175	33.0000	0.5249	0.6186
34.0000	0.4395	0.6181	34.0000	0.3906	0.6293
35.0000	0.3784	0.6177	35.0000	0.3174	0.6180
36.0000	0.1831	0.6182	36.0000	0.1831	0.6205
37.0000	0.0854	0.6181	37.0000	0.0854	0.6180
38.0000	0.0854	0.6183	38.0000	0.1221	0.6181
39.0000	0.1953	0.6180	39.0000	0.2075	0.6181
40.0000	0.3174	0.6182	40.0000	0.2930	0.6177
41.0000	0.4028	0.6180	41.0000	0.3418	0.6182
42.0000	0.4150	0.6175	42.0000	0.3784	0.6175
43.0000	0.3540	0.6181	43.0000	0.3174	0.6182
44.0000	0.2075	0.6181	44.0000	0.2808	0.6181
45.0000	0.2563	0.6181	45.0000	0.2686	0.6181
46.0000	0.1587	0.6180	46.0000	0.1587	0.6180
47.0000	0.1953	0.6181	47.0000	0.2075	0.6183
48.0000	0.2319	0.6182	48.0000	0.2686	0.6180
49.0000	0.2686	0.6184	49.0000	0.3174	0.6180
50.0000	0.3174	0.6177	50.0000	0.3052	0.6181

Appendix D   Comparison of accuracy in extracting mode 2, using the Gauss Windows (gausswin(200, α)) with different α for the seismic response data

α	ss_{12}	A_{12}	α	ss_{22}	A_{22}
1.0000	91.7114	0.4263	1.0000	90.6372	-0.6704
2.0000	86.2305	-2.3798	2.0000	84.9976	-0.8152
3.0000	76.5747	-0.5351	3.0000	75.4395	-0.7981
4.0000	64.7339	-1.2892	4.0000	63.8916	10.7795
5.0000	50.6958	-1.9187	5.0000	49.7070	-1.2140
6.0000	39.5142	-1.6058	6.0000	39.1357	-1.5343
7.0000	39.6973	-2.0673	7.0000	39.1602	-1.5070
8.0000	39.4409	-1.3629	8.0000	38.9038	-1.5263
9.0000	38.8306	-1.4071	9.0000	38.5864	-1.1170
10.0000	39.3066	-1.2214	10.0000	38.9038	-1.8022
11.0000	40.4663	-1.1372	11.0000	39.6118	-1.5941
12.0000	41.4429	-1.2769	12.0000	40.3809	-0.5614
13.0000	42.2119	-1.2830	13.0000	41.1377	-1.5728
14.0000	42.9443	-1.4596	14.0000	41.9067	-1.6374
15.0000	43.7256	-1.2812	15.0000	42.6270	-1.4603
16.0000	44.4092	-1.3194	16.0000	43.5059	-2.0506
17.0000	45.0684	-1.4493	17.0000	44.1406	-1.2682
18.0000	45.7397	-1.2797	18.0000	44.7388	-1.2838
19.0000	46.2646	-1.2510	19.0000	45.3125	-1.2108
20.0000	46.7041	-1.2278	20.0000	45.9229	-1.3586
21.0000	47.0215	-1.0167	21.0000	46.3867	-1.1404
22.0000	47.3755	-1.1702	22.0000	46.5698	-0.2799
23.0000	47.7661	-1.4454	23.0000	46.7896	-2.3064
24.0000	47.8394	-1.6406	24.0000	46.6797	-1.4186
25.0000	47.4243	-1.3741	25.0000	46.5820	1.9562
26.0000	47.4976	-0.8947	26.0000	46.3623	-2.4042
27.0000	47.9492	-1.8280	27.0000	46.5820	1.2799
28.0000	48.3643	-1.4294	28.0000	47.3145	-0.6479
29.0000	49.0967	-1.2022	29.0000	48.0713	-1.3071
30.0000	49.7803	-0.9696	30.0000	48.5840	-0.7519
31.0000	50.5981	-1.3730	31.0000	49.0845	-0.4065
32.0000	51.0864	0.1996	32.0000	49.5972	-1.9485

33.0000	51.5137	-0.7403	33.0000	50.2441	-0.8823
34.0000	52.0508	2.2309	34.0000	50.6470	-1.1551
35.0000	52.7466	-1.4933	35.0000	51.0620	-4.4867
36.0000	53.1128	-1.6642	36.0000	51.4771	-0.4716
37.0000	53.4058	-1.4596	37.0000	52.0874	-2.1939
38.0000	54.0894	-1.3000	38.0000	52.3193	-3.7253
39.0000	54.3213	-5.1957	39.0000	52.8320	-1.7630
40.0000	54.6143	-0.5843	40.0000	53.2593	-0.8927
41.0000	55.0537	-1.4624	41.0000	53.3936	-2.1962
42.0000	55.4565	-1.1751	42.0000	53.7354	-2.2707
43.0000	55.7129	-1.3812	43.0000	54.0649	3.6555
44.0000	56.0059	-1.5128	44.0000	53.9551	-1.3383
45.0000	56.1279	-1.1143	45.0000	54.4556	-1.6838
46.0000	56.0791	-1.2496	46.0000	55.0415	-1.8904
47.0000	56.5063	-0.5194	47.0000	55.1025	-4.8750
48.0000	56.9458	-1.2463	48.0000	55.0171	-1.6784
49.0000	56.8726	-2.7577	49.0000	55.6396	4.4695
50.0000	56.7993	-1.4991	50.0000	55.8960	-1.9587

Appendix E **Comparison of accuracy in extracting mode 2 when it is dominated, using the Gauss Windows (gausswin(200, α)) with different α, without moving average, for the free-vibration data**

α	ss_{12}	A_{12}	α	ss_{22}	A_{22}
1.0000	0.1831	-1.6077	1.0000	0.0244	-1.6179
2.0000	0.1953	-1.6177	2.0000	0.0244	-1.6181
3.0000	0.1465	-1.6228	3.0000	0.0122	-1.6184
4.0000	0.0610	-1.6184	4.0000	0	-1.6180
5.0000	0.0610	-1.6183	5.0000	0.0366	-1.6181
6.0000	0.0488	-1.6179	6.0000	0	-1.6180
7.0000	0	-1.6181	7.0000	0	-1.6180
8.0000	0	-1.6180	8.0000	0	-1.6180
9.0000	0	-1.6181	9.0000	0	-1.6180
10.0000	0	-1.6180	10.0000	0	-1.6180
11.0000	0	-1.6180	11.0000	0	-1.6180
12.0000	0	-1.6180	12.0000	0	-1.6180
13.0000	0.0122	-1.6180	13.0000	0	-1.6180
14.0000	0	-1.6180	14.0000	0	-1.6180
15.0000	0	-1.6180	15.0000	0	-1.6180
16.0000	0.0244	-1.6375	16.0000	0	-1.6180
17.0000	0	-1.6181	17.0000	0	-1.6180
18.0000	0	-1.6181	18.0000	0	-1.6180
19.0000	0	-1.6180	19.0000	0	-1.6180
20.0000	0	-1.6180	20.0000	0	-1.6180
21.0000	0	-1.6181	21.0000	0	-1.6180
22.0000	0	-1.6180	22.0000	0	-1.6180
23.0000	0.0122	-1.6180	23.0000	0	-1.6180
24.0000	0	-1.6180	24.0000	0	-1.6180
25.0000	0	-1.6180	25.0000	0	-1.6180
26.0000	0.0244	-1.6179	26.0000	0	-1.6180
27.0000	0.0244	-1.6178	27.0000	0	-1.6180
28.0000	0.0366	-1.6201	28.0000	0	-1.6180
29.0000	0	-1.6181	29.0000	0	-1.6180
30.0000	0.0122	-1.6181	30.0000	0	-1.6180

31.0000	0.0122	-1.6181	31.0000	0.0244	-1.6179
32.0000	0	-1.6180	32.0000	0	-1.6180
33.0000	0.0122	-1.6181	33.0000	0	-1.6180
34.0000	0.0122	-1.6180	34.0000	0	-1.6180
35.0000	0.0122	-1.6181	35.0000	0.0122	-1.6180
36.0000	0	-1.6180	36.0000	0	-1.6180
37.0000	0	-1.6180	37.0000	0	-1.6180
38.0000	0	-1.6180	38.0000	0	-1.6180
39.0000	0	-1.6180	39.0000	0	-1.6180
40.0000	0.0610	-1.6182	40.0000	0	-1.6180
41.0000	0	-1.6181	41.0000	0	-1.6180
42.0000	0	-1.6180	42.0000	0	-1.6180
43.0000	0	-1.6180	43.0000	0	-1.6180
44.0000	0	-1.6180	44.0000	0	-1.6180
45.0000	0	-1.6180	45.0000	0	-1.6180
46.0000	0	-1.6180	46.0000	0	-1.6180
47.0000	0	-1.6180	47.0000	0	-1.6180
48.0000	0	-1.6180	48.0000	0	-1.6180
49.0000	0	-1.6180	49.0000	0	-1.6180
50.0000	0.0122	-1.6181	50.0000	0	-1.6180

Appendix F Comparison of accuracy in extracting mode 2 when it is dominated, using the Gauss Windows (gausswin(200, 30)) with different i point moving average filter for the seismic response data

i	ss_{12}	A_{12}	i	ss_{22}	A_{22}
1.0000	17.2363	-1.5246	1.0000	16.7969	-1.5487
2.0000	20.4712	-2.1353	2.0000	19.9219	-1.5701
3.0000	19.3481	-1.5525	3.0000	18.4692	-1.7003
4.0000	24.6094	-1.6915	4.0000	23.9014	-1.8289
5.0000	15.9790	-1.4582	5.0000	15.1367	-1.5928
6.0000	24.0479	-1.5460	6.0000	23.1445	-2.8298
7.0000	19.9707	-1.5002	7.0000	19.1162	1.7629
8.0000	22.4121	-1.6411	8.0000	21.6553	-2.0103
9.0000	17.3340	-1.5581	9.0000	16.6748	-1.5767
10.0000	24.9268	-1.5136	10.0000	24.1211	-1.7462
11.0000	17.4805	-1.5390	11.0000	16.7969	-1.7384
12.0000	26.0620	-1.6034	12.0000	25.0000	-1.3098
13.0000	23.2056	-1.8386	13.0000	21.9971	-1.5775
14.0000	20.8496	-1.5247	14.0000	19.7510	-1.5294
15.0000	24.7314	0.6702	15.0000	23.5596	-1.2020
16.0000	20.0562	-1.3099	16.0000	18.9697	-1.6433
17.0000	27.6001	-1.5067	17.0000	26.2939	-1.5600
18.0000	18.4692	-1.5374	18.0000	17.6147	-1.4081
19.0000	24.6094	-1.6966	19.0000	23.3765	-1.5446
20.0000	15.6982	-1.6106	20.0000	14.4775	-1.6109
21.0000	24.5483	-1.5308	21.0000	23.6206	-2.4151
22.0000	25.8545	-1.5930	22.0000	24.4385	-1.6296
23.0000	30.5664	-1.5017	23.0000	29.1992	-2.2163
24.0000	30.2734	-1.7048	24.0000	29.0527	-1.5207
25.0000	23.7793	-1.8266	25.0000	22.3633	-1.5126
26.0000	30.4565	0.3170	26.0000	28.9429	-1.7204
27.0000	24.3530	-1.6622	27.0000	22.9858	-1.7408
28.0000	28.5034	-1.6858	28.0000	27.0508	-1.4215
29.0000	25.9766	-2.4759	29.0000	24.6826	-0.8717
30.0000	21.6309	-1.3963	30.0000	20.2393	-1.6763

31.0000	26.4893	-1.5515	31.0000	25.4272	-1.4986
32.0000	23.4741	-1.6427	32.0000	22.1436	-1.4969
33.0000	25.6348	-2.8061	33.0000	24.4141	-1.3691
34.0000	24.7192	-1.6516	34.0000	23.1812	-1.5644
35.0000	25.6714	-1.5865	35.0000	24.7681	-1.6301
36.0000	30.3955	-1.5298	36.0000	28.6987	-2.0356
37.0000	20.8130	-1.5885	37.0000	18.8843	-1.6125
38.0000	26.3550	-1.5303	38.0000	24.3408	-3.0815
39.0000	27.4414	-1.4616	39.0000	26.0376	-1.8689
40.0000	31.2500	-1.5324	40.0000	29.7241	-1.4418
41.0000	34.4604	-1.5616	41.0000	32.9712	-1.8826
42.0000	27.8442	-1.7264	42.0000	25.9888	-1.3502
43.0000	32.2266	-1.6010	43.0000	30.5420	-0.8341
44.0000	27.4780	-1.5912	44.0000	25.5249	-1.1993
45.0000	30.5420	-1.6092	45.0000	28.8574	-1.7159
46.0000	29.9316	-1.6537	46.0000	28.0151	-1.8944
47.0000	26.1597	-1.6087	47.0000	23.8281	-1.4488
48.0000	26.4893	-1.5376	48.0000	24.2065	-0.9596
49.0000	24.3286	-1.5565	49.0000	21.2646	-1.5625
50.0000	30.0171	-1.6133	50.0000	28.2471	-1.5548